ACS OMEGA

http://pubs.acs.org/journal/acsodf

Review

MoS_2-Based Nanocomposites for Photocatalytic Hydrogen Evolution and Carbon Dioxide Reduction

Bhagyalakshmi Balan, Marilyn Mary Xavier, and Suresh Mathew*

Cite This: *ACS Omega* 2023, 8, 25649−25673

Read Online

ACCESS | Metrics & More | Article Recommendations

ABSTRACT: Photocatalysis is a facile and sustainable approach for energy conversion and environmental remediation by generating solar fuels from water splitting. Due to their two-dimensional (2D) layered structure and excellent physicochemical properties, molybdenum disulfide (MoS_2) has been effectively utilized in photocatalytic H_2 evolution reaction (HER) and CO_2 reduction. The photocatalytic efficiency of MoS_2 greatly depends on the active edge sites present in their layered structure. Modifications like reducing the layer numbers, creating defective structures, and adopting different morphologies produce more unsaturated S atoms as active edge sites. Hence, MoS_2 acts as a cocatalyst in nanocomposites/heterojunctions to facilitate the photogenerated electron transfer. This review highlights the role of MoS_2 as a cocatalyst for nanocomposites in H_2 evolution reaction and CO_2 reduction. The H_2 evolution activity has been described comprehensively as binary (with metal oxide, carbonaceous materials, metal sulfides, and metal−organic frameworks) and ternary composites of MoS_2. Photocatalytic CO_2 reduction is a more complex and challenging process that demands an efficient light-responsive semiconductor catalyst to tackle the thermodynamic and kinetic factors. Photocatalytic reduction of CO_2 using MoS_2 is an emerging topic and would be a cost-effective substitute for noble catalysts. Herein, we also exclusively envisioned the possibility of layered MoS_2 and its composites in this area. This review is expected to furnish an understanding of the diverse roles of MoS_2 in solar fuel generation, thus endorsing an interest in utilizing this unique layered structure to create nanostructures for future energy applications.

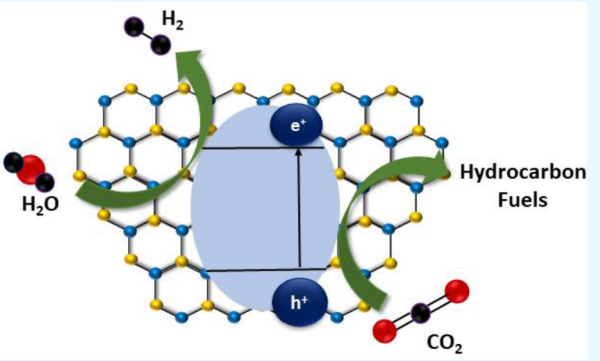

1. INTRODUCTION

Overusing fossil fuels, growing environmental pollution, and global climate change are the most significant challenges in this century. This crisis has emphasized developing renewable and clean energy sources for future purposes. One of the potential alternatives for this dilemma is solar energy. Semiconductor photocatalysis is a process that effectively converts solar energy to chemical energy. It is considered one of the most widely explored solar-fuel strategies for the photocatalytic splitting of water into H_2 and O_2 and the photocatalytic reduction of CO_2 into hydrocarbon fuels.[1−4] So far, noble metals, viz., Au, Pd, and Pt, are the most efficient catalysts for either H_2 evolution or CO_2 reduction reactions. However, over the past two decades, significant progress has been achieved in creating an efficient catalyst for H_2 evolution and CO_2 reduction utilizing non-noble metals, including metal oxides,[5−10] metal sulfides,[11,12] chalcogenides,[13,14] carbonaceous materials,[15,16] and carbides.[17−19] Among these, the discovery of materials having two-dimensional (2D) structures has been a significant triumph in developing and expanding the energy industry. Primarily, such a journey started with the invention of graphene in 2004 by Andre Geim and Kostya Novoselov.[20,21] Their outstanding properties significantly influence energy-related fields, such as solar cells, photo and electrocatalysis, light-emitting diodes (LEDs), transistors, and photodetectors.[22−27] Like graphene, layered transition metal dichalcogenides (TMDCs) were introduced as another class of 2D materials with intriguing properties that could potentially replace noble metals in catalytic applications. Molybdenum disulfide (MoS_2) mainly shows wide applications in various energy-related fields.[28−30] Most importantly, MoS_2-based nanocomposites have developed significantly in photocatalysis, such as pollutant degradation,[31,32] H_2 production,[33,34] and CO_2 reduction.[35,36] Therefore, we explore the advancement of nanocomposites based on MoS_2 in photocatalytic H_2 evolution and CO_2 reduction.

Received: March 29, 2023
Accepted: June 27, 2023
Published: July 12, 2023

2. PHOTOCATALYTIC HYDROGEN EVOLUTION REACTION (HER)

2.1. Basic Principles of HER. The overall photocatalytic splitting of H_2O to produce H_2 follows three basic steps. The first step is the electron−hole pair generation through photon absorption, which occurs inside the photocatalyst. Second-step involves the separation of charge carriers and their transport to the surface of the photocatalyst, and the third step constitutes the subsequent surface reduction of photoexcited electrons to produce hydrogen (Figure 1). Water splitting to produce H_2 is a thermodynamically uphill reaction, and the free energy associated with this process is 237.2 kJ mol^{-1}, corresponding to 1.23 eV. Therefore, the photocatalyst has a minimum band gap energy of 1.23 eV for water splitting, and the band gap should be lower than 3 eV for maximum solar energy utilization. Another criterion is related to the positions of the valence band (VB) and conduction band (CB) of the photocatalyst; the conduction band minimum (CBM) of the photocatalyst should be above the water reduction potential, and the valence band minimum (VBM) should be below the water oxidation potential.[37] Thus, this limitation of band gap is a significant problem associated with the low yield of H_2 production in most photocatalysts.

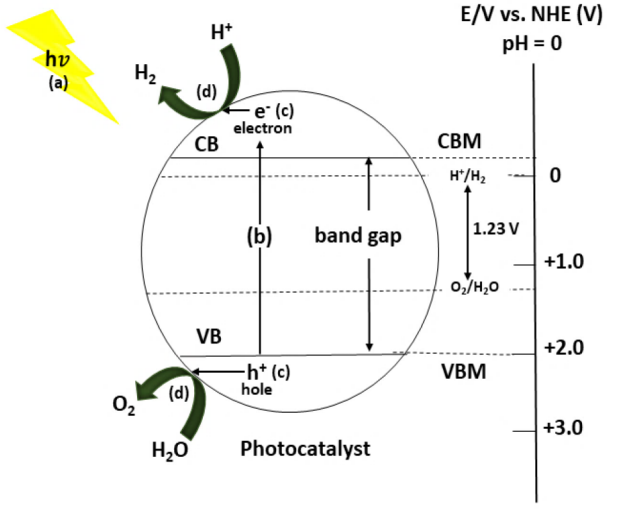

Figure 1. Schematic illustration of the sequences of photocatalytic H_2O splitting in a photocatalyst: (a) irradiation of light and photon absorption, (b) generation and separation of charge carriers, (c) migration of electron and hole to the surface of the photocatalyst, and (d) oxidation−reduction reactions on the surface to produce H_2 and O_2.

2.2. Structure and Properties of MoS_2. Hydrogen (H_2), having an energy density of 140 MJ kg^{-1}, is an ideal solution for future energy and environmental crises.[38−40] Since the pioneering discovery by Fujishima and Honda in 1972 through the photoelectrochemical splitting of H_2O, H_2 production via solar energy using semiconductor photocatalysts has received greater attention from researchers.[41,42] Further research is ongoing to produce highly active photocatalysts for photocatalytic H_2 evolution with high catalytic activity and lower overpotential. The development of nanocomposites of MoS_2 for photocatalytic H_2 generation is of great interest due to its excellent chemical stability, low cost, nontoxicity, and 2D-layered structure.[43−45]

It is well-known that bulk MoS_2 has a bandgap of 1.2 eV and has interestingly been explored as a lubricant, 2D transistor, and hydrodesulfurization catalyst. As shown in Figure 2a, it is composed of vertically stacked, weakly interacting layers held together by van der Waals interactions. In monolayer MoS_2, the Mo atoms are sandwiched between two layers of sulfur atoms with a thickness of 0.65 nm. On the basis of the atomic stacking order, MoS_2 has three structural polymorphs: 2H (two layers per repeat unit, hexagonal symmetry), 3R (three layers per repeat unit, rhombohedral symmetry), and 1T (one layer per repeat unit, tetragonal symmetry)[46,47] (Figure 2b).

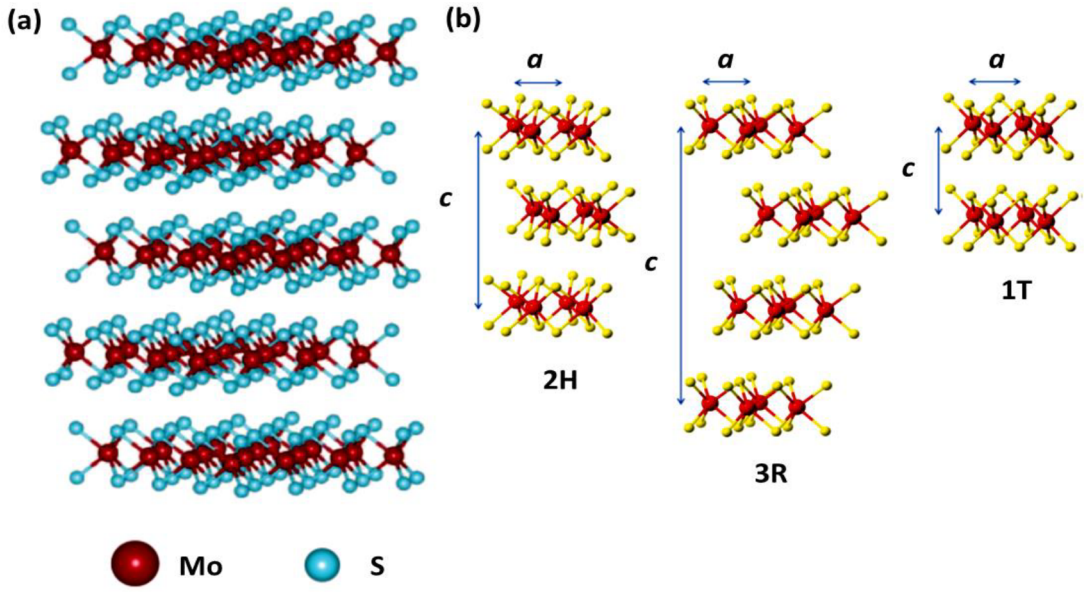

Figure 2. (a) Three-dimensional representation of the structure of a MoS_2 monolayer. Reproduced from ref 46. Copyright 2014 American Chemical Society (b) Schematic structural polytypes: including 2H, 3R, and 1T MoS_2 polytypes. Reproduced with permission from ref 44. Copyright 2016 Elsevier.

https://doi.org/10.1021/acsomega.3c02084
ACS Omega 2023, 8, 25649−25673

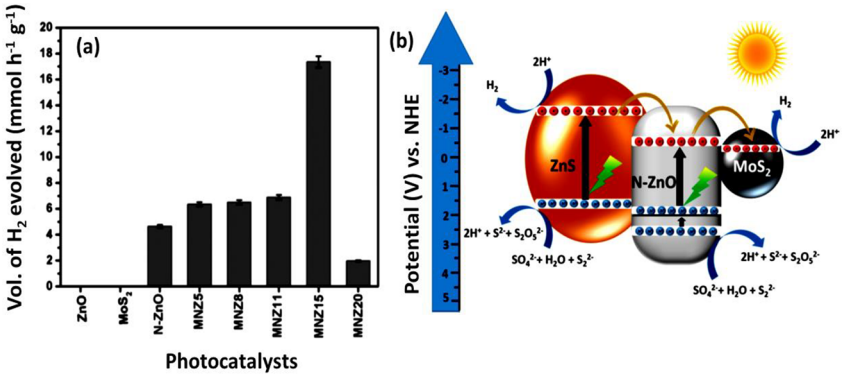

Figure 3. (a) Volume of H_2 generated using the N-ZnO-MoS_2 photocatalysts. (b) Schematic illustration of photocatalytic H_2 generation on the N-ZnO-MoS_2 heterostructure under natural sun light. Reproduced from ref 63. Copyright 2019 American Chemical Society.

MoS_2 has numerous intriguing properties due to its unique layered structure. Because of the antibonding state created by the interaction between molybdenum dz^2 and sulfur p_z orbital at the top of the valence band, MoS_2 exhibits excellent stability versus photocorrosion in solution. Previous research on bulk MoS_2 revealed that it would not be an effective HER catalyst during light illumination.[48,49] However, studies have demonstrated that the fabrication of nanostructured MoS_2 materials can considerably enhance HER activity, which is driven by several factors. For bulk MoS_2, the CB edge potential is positioned at −0.16 V, more than the H^+/H_2 redox couple (−0.41 V vs SHE, pH 7). As a result, it fails to satisfy the condition of water splitting. Alternatively, the CB edge potential tends to be −0.53 eV in monolayers, indicating the ability to reduce protons to generate H_2.[50,51] This kind of indirect-to-direct bandgap transition of MoS_2 was accomplished by decreasing the layer numbers, which resulted in an increase in bandgap from 1.2 eV (bulk MoS_2) to 1.9 eV (monolayer MoS_2), eliminating the potential barrier, and MoS_2 could be used as appropriate material for the water-splitting reaction.[47,52] Hinnemann et al. employed DFT calculations to determine the free energy of hydrogen adsorption (GH* on the MoS_2 edge) to find out the active edge sites of MoS_2 for the H_2 evolution reaction. The results demonstrated that GH* is significantly close to thermoneutrality, suggesting that MoS_2 could be an effective HER catalyst. This result was also confirmed experimentally by the electrochemical measurements of MoS_2 particles grown on graphite.[53] Bonde et al. made similar calculations and determined the free energy of adsorption on MoS_2 edges.[54] Nørskov's group has recently modified these values. On the basis of their findings, the suitable edge configurations correspond to Mo edges covered with 50% S having GH* = 0.06 eV instead of S being covered with 100% S having GH* = −0.45 eV.[55] Meanwhile, Jaramillo et al. provided experimental evidence for the role of MoS_2 edges in the HER reaction. They systematically produced different sizes of MoS_2 nanoclusters and correlated the electrochemical behavior and edge length of MoS_2 nanoclusters by STM analysis. The results show that the HER activity was associated linearly with many edge sites on the MoS_2 catalyst. Thus, the edge sites of MoS_2 were identified as active sites for the HER reaction.[56] Hence, the first part of this review focuses on 2D layered MoS_2-based nanocomposites as photocatalysts for H_2 evolution reactions. It envisages the unique role of MoS_2 in increasing the photocatalytic activity of different composites for future energy applications.

2.3. MoS_2-Based Composites for Photocatalytic Hydrogen Evolution Reaction.

2.3.1. MoS_2/Metal Oxide Composites. The fundamental issues associated with metal oxide as photocatalysts are the ultrafast charge recombination and photocorrosion within the photocatalysts. Various heterostructures have been developed to overcome these issues by combining metal oxides with MoS_2 and providing promising, low-cost, efficient catalysts.[57,58] The edges of 2D MoS_2 nanosheets have more catalytically active sites that show superior photocatalytic activity. This edge site activity can be further enhanced efficiently by suppressing the stacking of MoS_2 flakes. This modified edge-enriched ultrathin MoS_2 nanosheets uniformly embedded into yolk−shell structured TiO_2 exhibited excellent photocatalytic H_2 evolution. The composite shows an H_2-evolution rate of 2443 μmol g^{-1} h^{-1} than pure TiO_2 (247 μmol g^{-1} h^{-1}) with a PL lifetime of 5.17 ns. Since the energy differences between the CB of TiO_2 and MoS_2 are comparable, the electrons are more easily transferred from the excited TiO_2 to MoS_2 nanosheets. Because of their higher active sites and enriched edges, ultrathin MoS_2 nanoflakes potentially act as an electron acceptor rather than bulk MoS_2.[59] Using a plasma sputtering method, a thin layer (0.5 to 10 nm) of MoS_2 is selectively deposited on the top of anodic anatase TiO_2 nanotubes (TiNTs). It has been tested in an open-circuit for photocatalytic H_2 evolution reaction. Using solar simulator (100 mW/cm^2), a significant increase in H_2-evolution can be observed using a nominal 1 nm thick MoS_2 on the top of a 6 μm thick TiNTs layer. The band gap positions of the TiNTs/MoS_2 structure were tuned from 1.2, 1.3, and 1.8 eV for the deposition of 10, 3, and 1 nm MoS_2, respectively. Here, MoS_2 serves as a photosensitizer and as an H_2 evolution cocatalyst.[60]

Several studies have shown that engineered defects at the 2D MoS_2 nanosheet edges can enhance the photocatalytic H_2 evolution efficiency. Metal oxides can be combined with this defect-rich ultrathin form of MoS_2 nanosheets to improve light-harvesting efficiency and increase the photocatalytic H_2 evolution rate.[61] Zhu et al., for example, developed a series of MoS_2-TiO_2 catalysts for photocatalytic H_2-evolution via a simple ball-milling process using MoS_2 as a precursor. The recombination of photogenerated charge carriers decreased the photocatalytic performance of pure TiO_2. The H_2 evolution activity increases considerably with MoS_2 loading, reaching a maximum photocatalytic activity of 150.7 μmol h^{-1} for the optimum 4.0 wt % MoS_2-TiO_2 catalyst. The too-quick ball-milling process produces significantly more defective MoS_2

https://doi.org/10.1021/acsomega.3c02084
ACS Omega 2023, 8, 25649−25673

Table 1. Summarized List of Photocatalytic Hydrogen Evolution of MoS_2 with Metal Oxides and Carbonaceous Materials

photocatalyst	synthesis method	light source	amount of catalyst	sacrificial reagent	H_2 evolution activity	ref
yolk shell TiO_2/ultrathin MoS_2	hydrothermal	300 W Xe lamp	50 mg	80 mL aqueous solution contains 20 mL methanol	2443 μmol g^{-1} h^{-1}	59
TiO_2/MoS_2	ball-milling	300 W Xe lamp	0.2 g	100 mL of 15% mixed methanol-H_2O solution	150.7 μmol h^{-1}	62
N-ZnO/defect rich MoS_2	hydrothermal	natural sunlight	10 mg	50 mL aqueous solution contains 0.3 M Na_2S and Na_2SO_4	17.3 mmol g^{-1} h^{-1}	63
ZnO/MoS_2	hydrothermal	300 W Xe lamp	100 mg	100 mL aqueous solution contains 0.1 M Na_2S and 0.1 M Na_2SO_3	768 μmol g^{-1} h^{-1}	64
Zn-porphyrin MoS_2/ZnO	hydrothermal	300 W LED lamp	100 mg	100 mL aqueous solution of 0.02 M TEOA	75 μmol g^{-1} h^{-1}	65
Bi_2O_3/MoS_2	hydrothermal	300 W Xe lamp	25 mg	50 mL aqueous solution contains 0.02 mol L^{-1} TEOA	3075.21 μmol g^{-1} h^{-1}	67
CeO_2/MoS_2	hydrothermal	150 W Xe lamp	20 mg	20 mL aqueous solution of methanol	508.44 μmol h^{-1}	70
activated carbon/MoS_2	liquid phase reaction	30 W white light LED lamp	0.1 g	200 mL 10 vol % TEOA aqueous solution	872.3 μmol h^{-1}	72
g-C_3N_4/MoS_2	hydrothermal	300 W Xe lamp	20 mg	20 mL of H_2O-methanol (4:1 v/v) solution	1497 μmol g^{-1} h^{-1}	73
hollow g-C_3N_4/MoS_2	impregnation and sulfidation	300 W Xe lamp	20 mg	100 mL aqueous solution contains 10 vol % lactic acid	26.8 μmol h^{-1}	75
g-C_3N_4/MoS_2	impregnation method	300 W Xe lamp	0.1 g	120 mL of aqueous solution contains 25% methanol	23.10 μmol h^{-1}	76
g-C_3N_4/MoS_2	hydrothermal	300 W Xe lamp	50 mg	120 mL of aqueous solution contains 25% methanol	867.6 μmol g^{-1} h^{-1}	77
g-C_3N_4/MoS_2	hydrothermal	300 W Xe lamp	50 mg	250 mL 0.1 M TEOA aqueous solution	1155 μmol g^{-1} h^{-1}	78

structures, which is essential to the practical application of this simple, cost-effective, and sustainable method.[62] In addition to TiO_2, the coupling of MoS_2 with other metal oxide photocatalysts has also been investigated. Defect-rich MoS_2-nanosheets combined with nitrogen-doped ZnO nanorod composites has recently been developed.[63] Under solar light irradiation, an optimized heterostructure consisting of 15 wt % defect-rich MoS_2 nanosheets coated on N-ZnO (N-ZnO-MoS_2) exhibited the maximum H_2 evolution, 17.3 mmol h^{-1} g^{-1} (Figure 3a). The effective encapsulation of defect-rich MoS_2 nanosheets over N-ZnO nanorods resulted in a defect-induced interfacial contact region, contributing to increased photocatalytic activity. Figure 3b illustrates the pathway of enhanced photocatalytic H_2 evolution reaction. Under sunlight irradiation, the electron transfer occurs from the in situ generated ZnS to the conduction band of N-ZnO, followed by the defect-rich MoS_2 nanosheets. The defect-rich structure has several active edge sites with many exposed unsaturated "S" atoms that show a significant affinity for H^+ ions to produce H_2 during this reaction and boost visible light absorption. Using a simple hydrothermal approach, Yuan et al. investigated the effect of the interaction of MoS_2-nanosheet with ZnO nanoparticles.[64] Noble metals have replaced MoS_2 as a cocatalyst for many photocatalytic H_2 evolution reactions. For comparison, composites of ZnO with noble metals were also made.

Among these, Rh exhibited the maximum photocatalytic H_2 evolution rate of 153 μmol h^{-1} g^{-1}, around one-fifth of the 1 wt % MoS_2-ZnO composite photocatalyst (768 μmol g^{-1} h^{-1}). Hence, layered MoS_2 could be used as a substitute for noble metals in photocatalytic H_2 evolution reactions. Similarly, a noble metal-free visible light H_2 evolution was achieved through Zn-5, 10, 15, 20-tetrakis (4-carboxyphenyl)-porphyrin dye (Zn TCPP) sensitized MoS_2/ZnO heterostructures as a photocatalyst. The effect of MoS_2 loading on the photocatalytic activities of the Zn TCPP-MoS_2/ZnO hybrid system was investigated using triethanolamine (TEOA) aqueous solution as a sacrificial agent. The results suggested that, even without any noble metals, the as-prepared composite loaded with 0.5 wt % MoS_2 delivered an H_2 evolution rate of 75 μmol h^{-1} g^{-1}. The amount of MoS_2 loaded on the ZnO surface plays an essential role in trapping the conduction band electrons injected by the zinc porphyrin dye (ZnTCPP*), thereby suppressing the recombination of photogenerated charge carriers. This study provides insight into developing noble metal-free visible-light responsive ZnO-based photocatalysts using zinc porphyrin dyes as a light-harvesting material and MoS_2 as a cocatalyst.[65]

A photocatalytic H_2 evolution of ß-Tm^{3+}, Yb^{3+}: $NaYF_4/MoS_2$-Ta_2O_5 photocatalyst was reported by Shu et al. MoS_2 was deposited onto the surface of ß-Tm^{3+}, Yb^{3+}: $NaYF_4/Ta_2O_5$ nanocomposite as a cocatalyst. The presence of an up-conversion luminescence agent and MoS_2 cocatalyst could significantly increase the photocatalytic H_2 evolution rate of the Ta_2O_5 catalyst. Because of its outstanding electronic properties, MoS_2 provides more active sites to accept photogenerated electrons from the conduction band (CB) of Ta_2O_5 for H_2 evolution, reducing electron−hole recombination and increasing photocatalytic H_2 evolution activity of ß-Tm^{3+}, Yb^{3+}: $NaYF_4/MoS_2$-Ta_2O_5 catalysts.[66] A MoS_2/Bi_2O_3 Z-scheme heterojunction catalyst with rich oxygen vacancies was prepared in another study. The superior photocatalytic activity stemmed from oxygen vacancies that enhance the interfacial interaction between MoS_2 and Bi_2O_3.[67] Monolayer metal sulfides are promising for photocatalysis due to their excellent activity and high surface area. Especially their excellent charge carrier mobility shows high promise in photocatalysis.[68]

For the first time, catalytic H_2 production and pollutant degradation catalyzed by MoS_2 monolayers loaded on the m-$BiVO_4$ surface were studied using hybrid density functional calculations and long-range dispersion correction methods. Interfacial adhesion energy, binding energy, and equilibrium distance indicate that the association of MoS_2 monolayer with m-$BiVO_4$ (010) is a van der Waals interaction, resulting in a

https://doi.org/10.1021/acsomega.3c02084
ACS Omega 2023, 8, 25649−25673

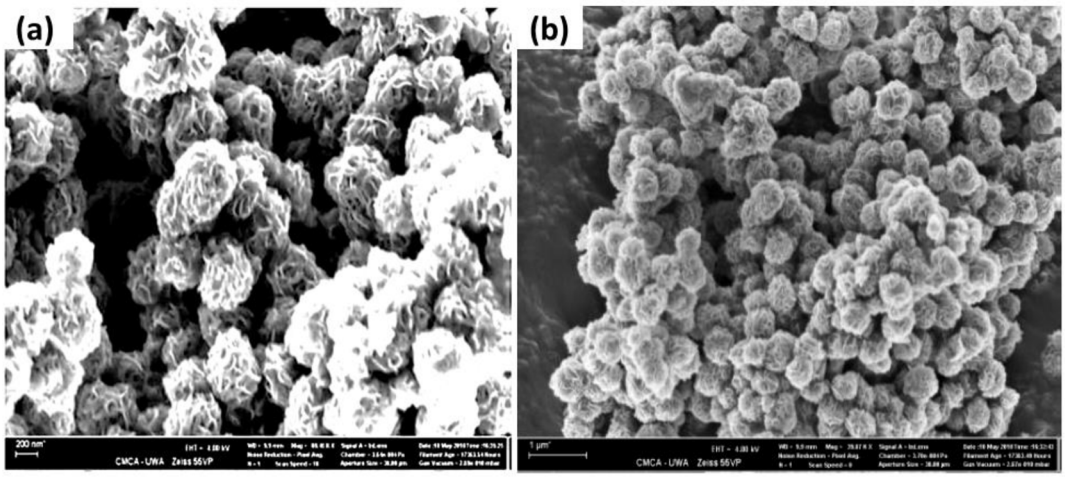

Figure 4. (a) SEM images of MoS_2. (b) 0.5% of MoS_2/gC_3N_4 photocatalyst. Reproduced with permission from ref 77. Copyright 2018 Elsevier.

high reduction capacity toward H_2 generation. With a high optical absorption coefficient, the monolayer of MoS_2 serves as a suitable electron acceptor, and more active sites can accept reactive species during the photocatalytic process.[69] Semiconductor photocatalysis through p-n heterojunctions is essential for improving future hydrogen storage. Swain et al. discovered a p-n heterojunction between p-type MoS_2 and n-type CeO_2 in a p-n heterojunction. The suggested p-n heterojunction method provides photoinduced charge transfer and separation. Following optimization of the overall experiment, it was discovered that the 2 wt % MoS_2/CeO_2 heterojunction nanocomposite has the most remarkable rate of H_2 evolution of 508.44 μmol h^{-1}.[70] Table 1 summarizes the different MoS_2/metal oxide composites, the synthesis method, and photocatalytic parameters to produce H_2 from the photocatalytic H_2O splitting.

2.3.2. MoS_2/Carbonaceous Materials. To enhance the catalytic efficiency of MoS_2 nanosheets, different layered carbon-based materials, including graphene, activated carbon, carbon nanofibers, and carbon nanotubes, have been incorporated. The resulting 2D/2D heterostructures with large contact areas will significantly benefit catalysis. Interfacial engineering between the layered heterojunctions as interface electron channels increases the HER performance.[71] Recently, Yin et al. reported an activated carbon/MoS_2 composite via a facile one-pot liquid phase reaction. The activity was mainly attributed to the in situ incorporation of activated carbon, resulting in an increased electrical conductivity due to the formation of thinner and smaller MoS_2 nanosheets.[72] A hydrothermal sulfurization and liquid phase exfoliation method was used to synthesize the modified gC_3N_4-MoS_2 heterojunction for the first time. An excellent system for exposing active edge sites to photochemical processes was obtained by adjusting the lateral diameters of MoS_2 nanosheets from 18 to 52 nm. The optimized structure with 20 wt % MoS_2 loading and a lateral size of 39 nm had the maximum photocatalytic H_2 activity of 1497 μmol h^{-1} g^{-1} and a quantum efficiency of 3.3% at 410 nm.

The density of MoS_2 edge sites created at the interface of the MoS_2/gC_3N_4 heterojunction is responsible for this increased HER activity. The MoS_2 nanosheets with a large fraction of surface edge sites enhance the electron transfer.[73] Inorganic molten salts offer a suitable platform for high 2D/2D heterostructures. A 2D/2D gC_3N_4-MoS_2 visible-light-driven photocatalyst is developed via simple pyrolysis of melamine and $(NH_4)_2MoS_4$ in a ternary molten LiCl-NaCl-KCl solution at 550 °C. The surface area of the composite was about 57 cm^2 g^{-1}, more than that of pure gC_3N_4. MoS_2 assembly suppresses the overgrowth of gC_3N_4-nuclei and enhances the synthesis of a hybrid structure with a greater porosity and H_2 evolution efficiency.[74]

A highly stable hollow carbon nitride nanosheet (HCNS) integrated MoS_2 was recently constructed by Zheng et al. for an H_2 evolution reaction. Applying lactic acid as a hole acceptor, the photocatalytic performance of MoS_2/HCNS nanocomposites for H_2 evolution was investigated. Upon 0.5 wt % MoS_2 loading, HCNS indicated an increase in the H_2 evolution rate of 26.8 μmol h^{-1}. The improved photocatalytic efficiency was ascribed to developing surface heterostructures across MoS_2 and HCNS, facilitating charge carrier separation and migration.[75] Ge et al. used a simple impregnation technique to produce MoS_2-gC_3N_4 composite photocatalysts. The maximum H_2 evolution rate of 23.10 μmol h^{-1} was obtained for the 0.5 wt % MoS_2-gC_3N_4 composite.[76] Using a simple hydrothermal process, a unique 3D flowerlike hexagonal 2H-MoS_2 was produced as thin stacked nanosheets, which were then combined with gC_3N_4 nanosheets of the same layered structure. The synthesized samples exhibited excellent photocatalytic and electrocatalytic activity with lower overpotential and substantial current densities. The SEM micrographs of pristine MoS_2 demonstrated 3D flowerlike nanostructures having a diameter of 400−600 nm and thicknesses of 10 nm. Remarkably, the nano platelike subunits are linked with one another to develop 3D flowerlike networks. It overcomes disordered stacking of MoS_2 layers by disclosing many active edge sites and increasing the specific surface area to decrease the diffusion pathway for both reactants and surface charges. The MoS_2/gC_3N_4 composites have a thinner and fluffier microstructure than pure gC_3N_4, showing the introduction and deposition of MoS_2 nanoflowers within the framework of gC_3N_4 nanosheets (Figure 4a,b). The 0.5% composition has the maximum photocatalytic activity of 867.6 μmol h^{-1} g^{-1}.

The photocatalytic activity was elevated to 2.8 times higher than pure gC_3N_4. Introducing a unique flowerlike MoS_2 structure boosted more increased and stable H_2 evolution activity. Several H^+ ions in the solution effectively bond to unsaturated active "S" atoms along the edges, converting them

https://doi.org/10.1021/acsomega.3c02084
ACS Omega 2023, 8, 25649−25673

into H_2.[77] Yuan et al. recently reported a 2D-2D MoS_2/gC_3N_4 photocatalyst having an H_2 evolution rate of 1155 μmol g^{-1} h^{-1}. The photoluminescence lifetime (PL) decreased as the concentration of MoS_2 increased, confirming that MoS_2 plays a crucial role in the effective separation of charge carriers.[78] The chemical vapor deposition (CVD) process was used to synthesize 3D edge-oriented graphene with an edge-rich MoS_2 nanoarray corresponding to gC_3N_4. The high conductivity and transparency of the 3D graphene layer provide a large exposed surface area for incorporating many photocatalysts, and developed 3D graphene/E-MoS_2 structures exhibit superior optical and electrical characteristics. The maximum H_2 evolution activity of 2232.7 μmol g^{-1} h^{-1} was achieved under white light irradiation.[79] Binary composites of MoS_2-carbon nitride (MoS_2-CN) have recently been found as a substrate for piezo-photocatalytic hydrogen evolution reactions. The structure of the MoS_2 on CN significantly impacts the piezoelectric activity of the binary composites. The MoS_2 nanosheet acts as a piezo potential generator to induce an electric field on CN; thus, the recombination of the charge carriers is inhibited under low-frequency vortex vibration.[80] Table 1 outlines the various MoS_2/carbonaceous composites and the synthesis methods and photocatalytic parameters used to produce H_2 by photocatalytic water splitting.

2.3.3. MoS_2/Metal Sulfides. Many metal chalcogenides, such as CdS, In_2S_3, Bi_2S_3, and CuS, have narrow band gaps and excellent absorption in the visible light range, making them suitable candidates for photocatalytic H_2O splitting to release hydrogen.[81−83] However, metal sulfides also had significant drawbacks, such as fast electron−hole pair recombination and serious photocorrosion in photocatalysis. MoS_2, as a catalyst in association with typical metal chalcogenides, can increase solar energy absorption in the visible range. For example, Li et al. demonstrated cost-effective and efficient photocatalysis based on MoS_2 and CdS nanospheres.[84] MoS_2 is intimately formed on CdS and has an unusually high H_2-evolution activity of 37.31 mmol g^{-1} h^{-1}.

The agglomeration-resistant structure, low overpotential, and the large number of active sites of MoS_2 contribute to the exceptional photocatalytic efficiency of these heterostructures.[84] The HER activity of MoS_2 nanosheets is linked to the active "S" atoms on the exposed edges rather than the S atoms presented on the basal planes, and this can be increased further by reducing the layer numbers of MoS_2.[85] In particular, CdS-MoS_2 hybrids have attracted more attention, and several heterogeneous photocatalysts have been generated from CdS nanocrystals by integrating with MoS_2 cocatalysts. For example, few-layered MoS_2 nanosheets loaded with CdS nanorods produce a high H_2 evolution rate (1009 mmol h^{-1} g^{-1}) with an apparent quantum efficiency (AQE) of 71% at 420 nm. The few-layer MoS_2 edges attached to CdS contain the more active sites, minimizing the distance and resistance of the transfer of electrons from the basal plane for the H_2 evolution process.[86]

Ma et al. also developed a 2D-2D CdS/MoS_2 heterojunction for photocatalytic H_2 evolution reaction. Under visible light, the heterojunctions could attain hydrogen evolution activity of 1.75 mmol g^{-1} h^{-1}, using an aqueous solution of sulfide and sulfate, and this became 2.03 times greater than pure CdS NSs. The increased activity can be due to the loading of MoS_2 NSs, which effectively promotes the separation of charge carriers.[87] A possibility of photocatalytic H_2 evolution using biomass-derived sacrificial reagents such as glucose has been applied to a series of flowerlike CdS/MoS_2 binary heterostructure composites. After 900 min of continuous testing, the 40% CdS/MoS_2 catalyst achieved the maximum H_2 evolution rate (55.0 mmol g^{-1} h^{-1}) and maintained high stability. The synergistic interaction of CdS and MoS_2 facilitates effective charge carrier separation. Furthermore, glucose performed as a better sacrificial agent, creating more protons during photocatalysis.[88] Doping of MoS_2 with heteroatoms is a simple and effective approach for producing an excellent catalyst for H_2 production from water splitting. A Zn-doped few-layered MoS_2 on the surface of CdS was reported. The doped MoS_2 material was demonstrated to be a good cocatalyst for enhancing the photocatalytic activity of CdS. It also facilitates photoinduced charge transfer by providing many active edge sites for catalytic reactions and increasing long-term stability for useful applications. The optimized structure (6 wt % Zn-MoS_2) shows the maximum catalytic activity of 241 mmol h^{-1} g^{-1}, which is ∼75 times more than pure CdS.[89]

Similarly, Guo et al. synthesized the nickel subsulfide Ni_3S_2/MoS_2 heterostructure. The Ni_3S_2 nanostructures were developed on Ni foam via a sulfuration approach by the CVD method, and MoS_2 was formed along with the Ni_3S_2 nanostructures via a hydrothermal process. After synthesizing, the MoS_2 achieved direct interaction with the Ni_3S_2 structure, resulting in effective interfacial interaction. The hybrid enhances broadband absorption covering 300 to 800 nm, yielding a significant increase in hydrogen evolution (540.75 μmol g^{-1} h^{-1}).[90] Zhao et al. synthesized CdS nanorods with MoS_2 nanosheets, and the composite achieved an H_2 production rate of 63.71 and 71.24 mmol g^{-1} h^{-1} in visible light and stimulated sunlight irradiation, respectively. The resulting heterojunction effectively separates photogenerated holes and electrons. Decorating CdS and MoS_2 helped to reduce the photocorrosion of CdS nanorods by stabilizing the sulphions.[91] Similar results were obtained in another CdS/MoS_2 heterojunction.[92]

Multicomponent sulfides form heterostructures with MoS_2 received considerable attention for applications in photocatalytic hydrogen production.[93,94] By adding a transition metal into the CdS solid solution, photocorrosion of CdS can be eliminated and transition metal doped CdS can be formed. Among these, $Cd_xZn_{1-x}S$ takes more attention due to its excellent photocatalytic activity.

By combining with MoS_2, a new $Cd_xZn_{1-x}S/MoS_2$ heterojunction was synthesized by an electrostatic self-assembly method.[95] Similar results were also obtained for a 2D/2D $ZnIn_2S_4/MoS_2$ composite, achieving a H_2 evolution rate of 221.71 μmol h^{-1} was achieved under visible light irradiation. The close contact of $ZnIn_2S_4$ with MoS_2 offers several channels for carrier migration. Furthermore, the active S atoms at exposed edges of MoS_2 give more active sites for proton reduction.[96] Whereas Chand et al. adopted a two-step process including hydrothermal and simple chemical methods to fabricate MoS_2-$ZnIn_2S_4$ composites. The H_2 production rate was also increased by adding MoS_2 as a cocatalyst. MoS_2 is used as an oxidation catalyst to strengthen the oxidation half-cell reaction and synchronously strengthen the reduction half-cell reaction; thus, the overall photocatalytic H_2 evolution is enhanced.[97]

Many other reports have been published incorporating layered MoS_2 with ternary chalcogenides. Hexagonal $ZnIn_2S_4$ has received more attention due to its structural similarity with MoS_2. It is facile to develop an intimate 2D/2D $ZnIn_2S_4/MoS_2$

https://doi.org/10.1021/acsomega.3c02084
ACS Omega 2023, 8, 25649−25673

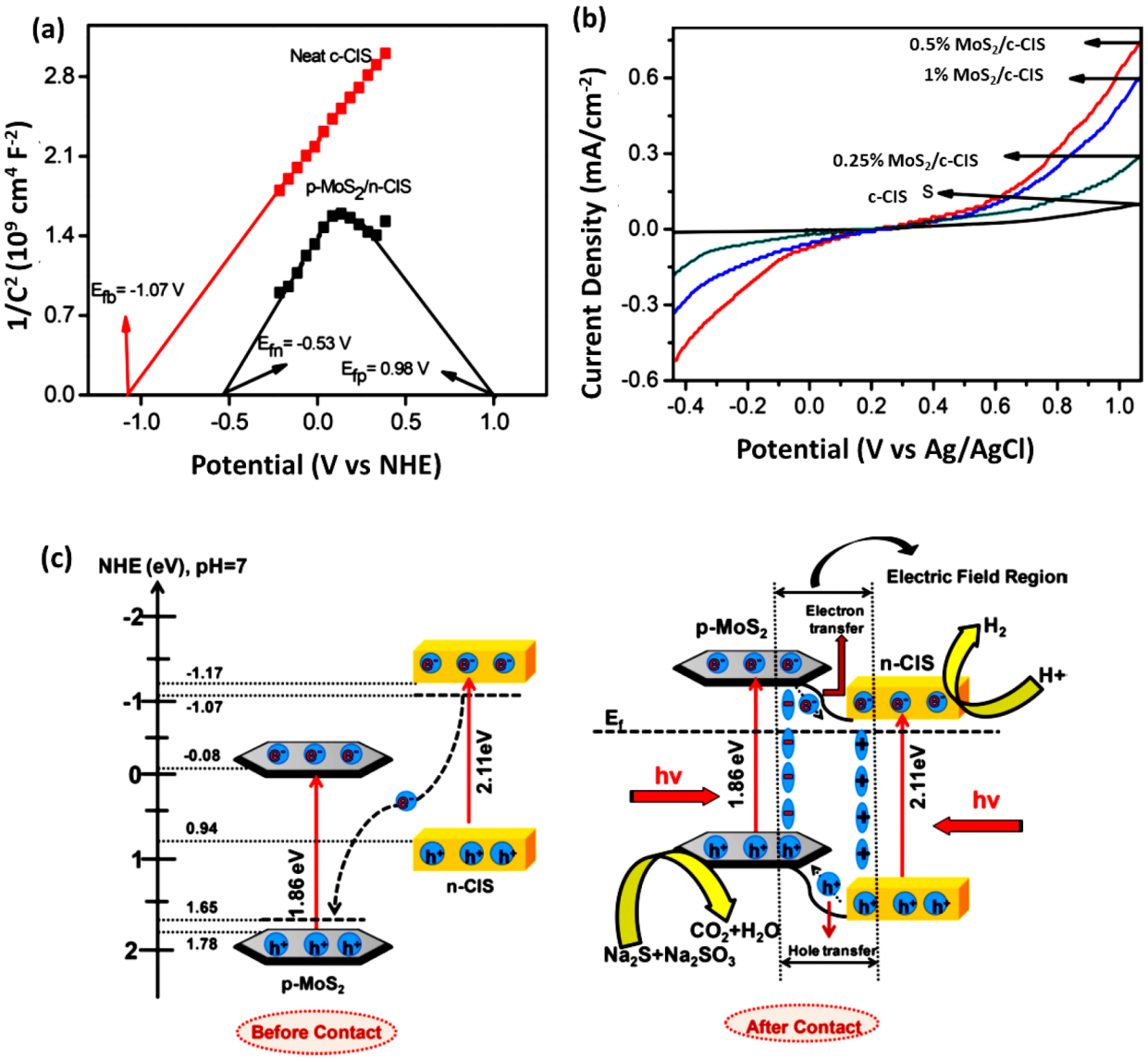

Figure 5. (a) Mott−Schottky plots of pure c-CIS and 0.5% MoS_2/c-CIS. (b) LSV curves of pure c-CIS and different MoS_2/c-CIS composites. (c) Possible charge transfer pathway for H_2 evolution by p−n junction mechanism. Reproduced from ref 105. Copyright 2018 American Chemical Society.

heterojunction by growing a layer of MoS_2 on the hexagonal $ZnInS_4$ surface. The CB position of MoS_2 was less negative than that of $ZnIn_2S_4$, resulting from the direct migration of photogenerated electrons possible through $ZnIn_2S_4$ to MoS_2.

The optimized 5% MoS_2/$ZnIn_2S_4$ composition exhibits a hydrogen production rate of 3891.6 μmol g^{-1} h^{-1}.[98] Huang et al. adopted a two-step hydrothermal method to construct the $ZnIn_2S_4$/MoS_2 composite. The interaction of MoS_2 can effectively promote electron−hole separation and extends the photocatalytic lifetime.[99] For the first time, a solvothermal process was adopted for the controlled growth of $ZnIn_2S_4$ nanosheets on few-layered MoS_2 slices to construct the MoS_2/$ZnIn_2S_4$ hybrid. The exfoliated 2D platform framework of MoS_2 slices can be an excellent supporting medium for the in situ growth of $ZnIn_2S_4$ nanosheets, enhancing interfacial charge transfer and minimizing self-agglomeration.[100] Other reports also showed the highly enhanced photocatalytic performance for the H_2-evolution of $ZnIn_2S_4$/MoS_2 composites.[101,102]

The $ZnIn_2S_4$/MoS_2 composite was synthesized using an environmentally friendly biomolecule-assisted microwave heating method. Using visible light irradiation, a $ZnIn_2S_4$/MoS_2 composite having an optimized weight percentage of MoS_2 was used to reduce harmful Cr (VI) ion to Cr (III) ion.

Furthermore, even following three cyclic tests, this catalyst demonstrated high stability. The $ZnIn_2S_4$ and MoS_2 combine to produce a type II heterostructure responsible for the increased activity.[103] Similarly, flowerlike p-MoS_2/n-$MgIn_2S_4$ hybrids were synthesized and studied for photocatalytic efficiency in H_2-evolution and N_2-reduction. By inducing an internal electric current at the interface of two photocatalysts, the p-n heterojunction provides an excellent potential for separating photogenerated charge carriers. MoS_2 nanosheets provide many exposed active sites through S−S bonding on the edges and offer efficient excitons separation.[104] Swain et al. developed another type II heterostructure with excellent charge separation efficiency. A set of roselike p-MoS_2 nanoflowers are decorated with n-type cubic $CaIn_2S_4$ (c-CIS)

https://doi.org/10.1021/acsomega.3c02084
ACS Omega 2023, 8, 25649−25673

Table 2. Summarized List of Photocatalytic Hydrogen Evolution of MoS_2/Metal Sulfide Composites and MoS_2/MOFs Composites

photocatalyst	synthesis method	light source	amount of catalyst	sacrificial reagent	H_2 evolution activity	ref
CdS/MoS_2	hydrothermal	300 W Xe lamp	20 mg	80 mL aqueous solution contains 8 mL lactic acid	37.31 mmol g^{-1} h^{-1}	84
CdS/MoS_2	hydrothermal	300 W Xe lamp	20 mg	100 mL aqueous solution contains lactic acid	1009 mmol g^{-1} h^{-1}	86
CdS/MoS_2	hydrothermal	300 W Xe lamp	50 mg	80 mL aqueous solution contains 0.5 mol L^{-1} Na_2S and 0.5 mol L^{-1} Na_2SO_3	1.75 mmol g^{-1} h^{-1}	87
CdS/MoS_2	hydrothermal	300 W Xe lamp	0.1 g	100 mL aqueous solution contains 0.1 M glucose	55 mmol g^{-1} h^{-1}	88
Ni_3S_2/MoS_2	CVD and hydrothermal	150 W Xe lamp	0.05 g	40 mL distilled H_2O contains 0.1 mol L^{-1} Na_2S and 0.1 mol L^{-1} Na_2SO_3	540.75 μmol g^{-1} h^{-1}	90
$ZnIn_2S_4/MoS_2$	electrostatic self-assembly	visible light	–	36 mL deionized H_2O + 4 mL lactic acid	4.97 mmol g^{-1} h^{-1}	93
$ZnIn_2S_4/MoS_2$	wet chemical method	300 W Xe lamp	25 mg	90 mL DIW H_2O + 10 mL TEA	8898 μmol g^{-1} h^{-1}	94
$ZnIn_2S_4/MoS_2$	solvothermal	300 W Xe lamp	80 mg	100 mL aqueous solution contains 0.35 M Na_2S and 0.25 M Na_2SO_3	3891.6 μmol g^{-1} h^{-1}	98
p-MoS_2/n-$ZnIn_2S_4$	hydrothermal	150 W Xe lamp	20 mg	100 mL aqueous solution contains 0.35 M Na_2S and 0.25 M Na_2SO_3	320.2 μmol h^{-1}	102
$ZnIn_2S_4/MoS_2$	hydrothermal	150 W Xe lamp	0.1 g	100 mL aqueous solution contains 0.35 M Na_2S and 0.25 M Na_2SO_3	200.1 μmol g^{-1} h^{-1}	103
$MgIn_2S_4/MoS_2$	hydrothermal	150 W Xe lamp	20 mg	20 mL aqueous solution contains 0.35 M Na_2S and 0.25 M Na_2SO_3	570.8 μmol h^{-1}	104
$CaIn_2S_4/MoS_2$	hydrothermal	150 W Xe lamp	20 mg	20 mL aqueous solution contains 0.025 M Na_2S and 0.025 M Na_2SO_3	602.35 μmol h^{-1}	105
MoS_2-MOF/Co_3O_4	hydrothermal	300 W Xe lamp	10 mg	15% (v/v) TEOA (30 mL) aqueous solution	629.75 μmol	106
MoS_2@Cd-MOF	solvothermal	300 W Xe lamp	30 mg	150 mL aqueous solution contains 35 mM Na_2S and 18 M Na_2SO_3	5587 μmol g^{-1} h^{-1}	108
$Cu_{0.9}Co_{2.1}S_4$@MoS_2	hydrothermal	300 W Xe lamp	–	aqueous solution contains TEOA	40156 μmol g^{-1} h^{-1}	110

micro flowers incorporating different amounts of MoS_2. Highly dispersed MoS_2 nanoflowers with more active edge sites provided the platform for growing $CaIn_2S_4$, resulting in a hierarchical network (MoS_2/c-CIS) with intimate contact. The p-n heterojunction character of the composite is revealed by electrochemical studies such as Mott–Schottky analysis and LSV curves. The lower slope of 0.5 wt % p-MoS_2/n-$CaIn_2S_4$ compared to pure $CaIn_2S_4$ indicated the increased donor density capacity, which was the primary source of the photocatalytic performance (Figure 5a). When the potential was applied, pure c-CIS showed a very low photocurrent, i.e., 0.09 mA, although all composites showed a significant photocurrent. The plot is asymmetrical in forward and reversed biasing (Figure 5b). The modified photocatalysts comprising 0.5 wt % p-MoS_2/n-$CaIn_2S_4$ had a higher H_2 generation rate of 602.35 μmol h^{-1}, having photocurrent densities of 0.743 mA cm^{-2}. The type II heterojunction photocatalyst was developed to improve charge separation effectiveness by shifting electrons from the upper Fermi level of n-type c-CIS to the lower Fermi level p-type MoS_2 (Figure 5c).[105] Table 2 outlines the various MoS_2/metal sulfides composites and the synthesis methods and photocatalytic parameters used to produce H_2 by photocatalytic water splitting.

2.3.4. MoS_2/Metal–Organic Frameworks (MOFs). Metal–organic frameworks (MOFs), a new class of porous and crystalline materials exhibiting massive coordination centers, have found significant applications in photocatalysis.[106,107] The photocatalytic activity of MoS_2 in water splitting for H_2 evolution can be enhanced by constructing heterogeneous interfaces with MOFs or MOF-derived metal oxides or sulfides. The sulfurization of the core–shell MoS_2@Cd-MOF constructed a new CdS/MoS_2 heterojunction. The CdS/MoS_2 presents uniform loading of CdS nanoparticles on the MoS_2 flowers. The composite exhibited a higher specific surface area of 78 m^2 g^{-1}, and the optimized CdS/MoS_2 heterojunction showed an average H_2 evolution rate of 5587 μmol g^{-1} h^{-1}. In the heterojunction, the conduction band minimum of MoS_2 is lower than that of CdS, so the photoexcited electrons transferring from CdS to MoS_2 become possible. The MoS_2 was a cocatalyst to trap photoexcited electrons and holes and improve photocatalytic activity.[108]

MoS_2 combined with terephthalic acid to form MoS_2-MOF and Co_3O_4 was deposited on these catalytic surfaces in methanol solution under light irradiation to form a MoS_2-MOF/Co_3O_4 photocatalyst. MoS_2-MOF constitutes a new type of catalyst that could provide a large specific surface area, pore size, and active sites to improve electron transport efficiency. The deposition of Co_3O_4 further accelerates the charge separation. The MoS_2-MOF structure appears as a leaf, and Co_3O_4 is structured into this system as a venation. This catalytic system has an excellent fluorescence quenching rate and lifetime, and photocatalytic hydrogen evolution reached 629.75 μmol using an eosin Y-sensitized system; this is a successful example of preparing an organic framework composed of metal sulfides as an H_2 evolution photocatalyst.[106] A simple hydrothermal approach developed a unique 3D nanofibrous aerogel-based MoS_2@Co_3S_4 composites. The heterojunction showed an exceptional H_2-evolution activity of 228.2 μmol g^{-1} h^{-1} and delivered excellent photocatalytic dye degradation toward Cr (VI), sulfamethoxazole, and bacteria.[109] A bimetallic metal–organic frameworks catalyst was coupled with MoS_2 forming a heterojunction of

https://doi.org/10.1021/acsomega.3c02084
ACS Omega 2023, 8, 25649–25673

the composition $Cu_xCo_{3-x}S_4$@MoS_2. After optimization, the flowerlike $Cu_{0.9}Co_{2.1}S_4$@MoS_2 catalyst delivered 40156 μmol g^{-1} h^{-1} of visible light H_2 production. These structures of $Cu_{0.9}Co_{2.1}S_4$@MoS_2 hybrid can fully expose the catalytic sites and maintain structural stability over a long period. The photocatalytic mechanism sensitized by eosin Y (EY) proceeds via a reductive electron transfer process. TEOA reductively quenches the excited EY molecules to produce EY*. Subsequently, electrons were transferred from the EY* molecule to the conduction band of $Cu_{0.9}Co_{2.1}S_4$@MoS_2, where the protons are reduced to form molecular H_2 (Figure 6a). The stability of the photocatalyst was retained steadily

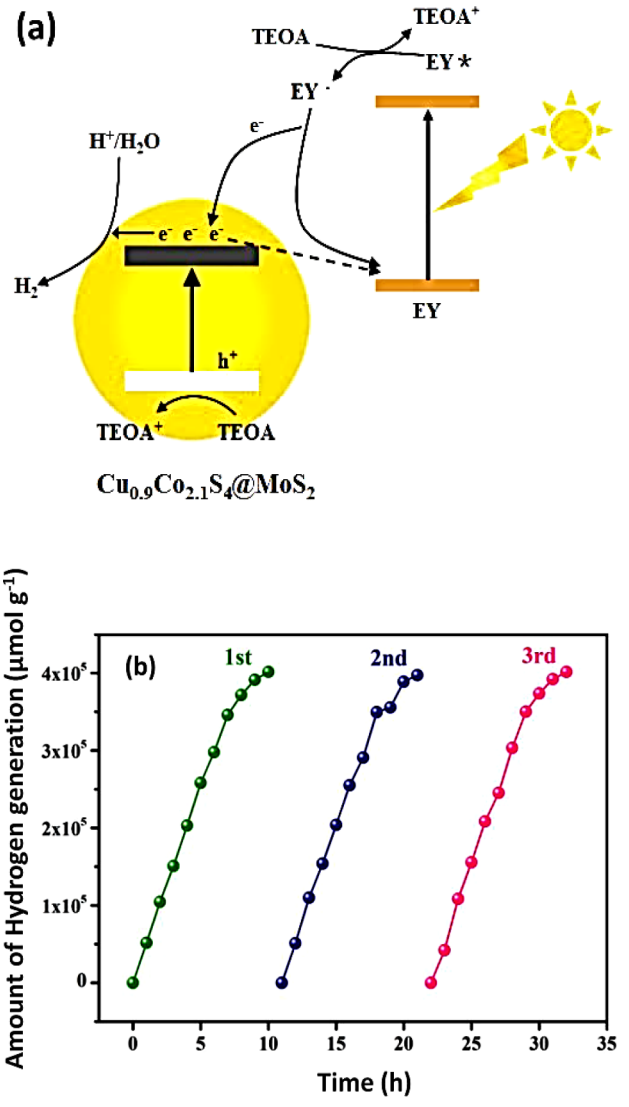

Figure 6. (a) Photocatalytic process for H_2 production on $Cu_{0.9}Co_{2.1}S_4$@MoS_2 photocatalyst using visible-light irradiation. (b) Stability tests of $Cu_{0.9}Co_{2.1}S_4$@MoS_2 in hydrogen evolution for three cycles under visible irradiation. Reproduced from ref 110. Copyright 2019 American Chemical Society.

after three consecutive cycles with an apparent quantum efficiency of about 3.2% (Figure 6b)[110] (Table 2). A MOF-199 modified MoS_2 heterojunction was reported by Qiao et al. to achieve high H_2 evolution via water splitting (626.3 μmol g^{-1} h^{-1}). The synthesized MOF/MoS_2 composites show the combined properties of MoS_2 and MOF; thus, the active sites can be significantly enhanced. Here the MOF-199 acts as a photosensitizer to assist MoS_2 in harvesting visible light by transferring photoexcited electrons to MoS_2.[111]

2.3.5. Ternary Composites of MoS_2. For photocatalytic H_2 evolution processes, MoS_2-based ternary materials have received considerable interest. Because of its numerous active sites and efficient separation of charge carriers, the MoS_2 ternary systems produce more H_2 than binary composites.[112,113] Zhu et al. has synthesized a ternary CeO_2@MoS_2/gC_3N_4 catalyst with excellent photocatalytic performance for H_2 production. The optimized 0D/2D composite produced a short and efficient multielectron transfer mechanism. The H_2 evolution rate achieved 65.4 μmol/h, roughly 8.3 and 17.5-fold higher than pure gC_3N_4 and CeO_2. The composite also exhibited an extended quantum efficiency of 10.35% at a wavelength of 420 nm.[114] Transition metal doping (Co) of MoS_2 effectively tunes the geometry and electronic structure for enhancing HER activity. A ternary $CoMoS_2$/rGO/gC_3N_4 was constructed by a solvothermal method. The synergistic effect between the nanosheets of gC_3N_4, rGO, and Co-doped MoS_2 enhances the HER activity rate to 684 μmol g^{-1} h^{-1}. The enriched electrons on $CoMoS_2$ with abundant active sites and lower atomic hydrogen absorption energy demonstrated high charge separation efficiency for reducing the protons to H_2.[115] In another study, a multifunctional ternary photocatalyst of MoS_2 was introduced by Kumar et al. They developed a photocatalytic and electrocatalytic H_2 production reaction for the ternary ZnO/MoS_2/RGO heterojunction. As shown in Figure 7a, H_2 evolution increases with increasing the MoS_2-RGO content. The optimized composition achieved the highest H_2 evolution (28.616 mmol g^{-1} h^{-1}). Because it comprises a layered structure containing exposed S atoms at its edge sites with a high affinity toward H^+ ions, the nanosized MoS_2 facilitates H_2 evolution (Figure 7b). During HER reaction, ZnO dissolves in an alkaline sulfide solution and the in situ-generated ZnS enhances interfacial charge transport to MoS_2 and RGO. The photocatalytic process also indicates that the synergistic effect of RGO-MoS_2 nanosheets and in situ formed ZnS efficiently reduce charge recombination in ZnO and significantly accelerates the H_2 evolution reaction (Figure 7c).[116] In another system, a noble metal-free heterostructured WS_2-MoS_2 integrated on CdS nanorods served as active sites for H_2 production. By accelerating the photoinduced charge transfer and reducing electron−hole recombination, the WS_2-MoS_2 heterostructure ultrathin nanosheets became an efficient cocatalyst for enhancing the photocatalytic hydrogen evolution rate.[117] CdS nanospheres with MoS_2 and NiP ternary nanohybrids were synthesized for the first time by using a hydrothermal process and a MOF-templated approach. The composite has a high photocatalytic H_2 evolution capacity of 72.76 mmol h^{-1} g^{-1} under optimum conditions.[118]

Yu et al. described a biomolecule-assisted synthesis of CdS/MoS_2/graphene hollow spheres. L-Cysteine worked as a sulfur source and was important for the self-assembly of the graphene structure to produce the ternary heterostructure. The CdS/MoS_2 heterojunction developed by in situ MoS_2 growth offers better contact. It allows more photogenerated electrons in CdS to move to the MoS_2 layer and combine with H^+ to produce H_2 at considerably lower overpotentials.[119] Similar results were obtained when MoS_2 was modified with CdS and PANI.[120] A ternary structure recently comprised of MoS_2/SiO_2/GO was reported as a photocatalytic degradation and H_2 evolution

https://doi.org/10.1021/acsomega.3c02084
ACS Omega 2023, 8, 25649−25673

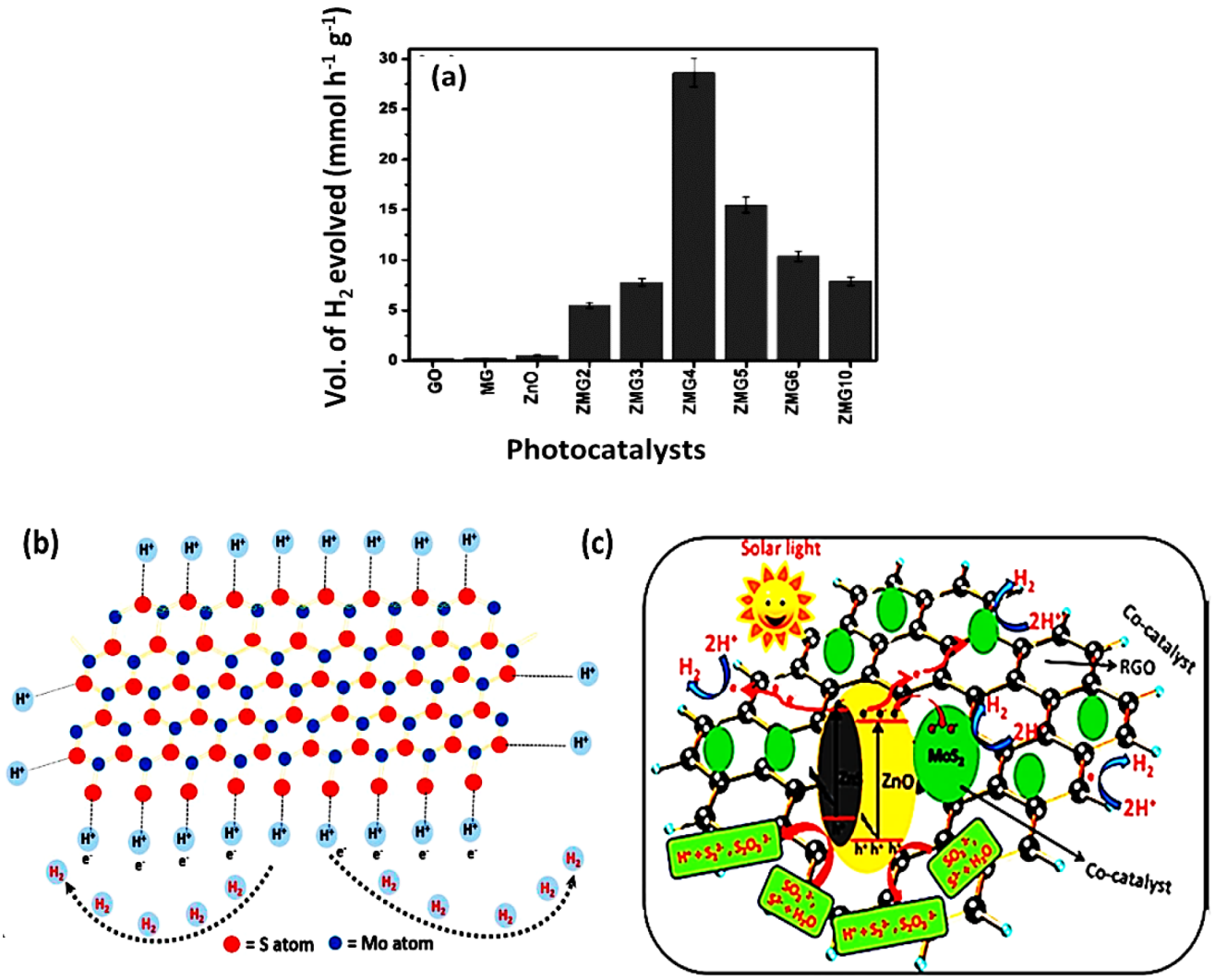

Figure 7. (a) H_2 volume evolved in various ternary ZnO/MoS_2/RGO photocatalysts. (b) Layered structure of nanosized MoS_2 showing exposed edges of sulfur atoms for H^+ ions in aqueous solution for HER performance. (c) A plausible mechanism for enhanced electron transfer across the ZnO-MoS_2-RGO heterojunction under solar irradiation using Na_2S-Na_2SO_3 as a sacrificial reagent. Reproduced with permission from ref 116. Copyright 2017 Wiley.

catalyst. The as-synthesized lotuslike ternary photocatalyst has a suitable energy band structure for removing cotton pulp black liquor (CPBL) and simultaneously produces H_2 (233.4 μmol). The loading of MoS_2 onto this SiO_2/GO structure dramatically improves the dispersion and specific surface area of MoS_2, endowing its superior photocatalytic activity.[121] As an excellent noble metal-free photocatalyst for H_2 generation, ternary MoS_2/ZnCdS/ZnS dual nanocomposites were fabricated. The material produces H_2 at a 79.3 mmol g^{-1} h^{-1} rate and an apparent quantum yield of 47.9 at 420 nm. MoS_2 has a higher specific perimeter and many active sites and easily separates and transports electron−hole pairs with enhanced photocatalytic performance.[122] A chemical vapor deposition (CVD) method was adopted to construct a novel MoO_2/MoS_2/TiO_2 ternary structure. Here few-layered MoS_2 nanoflakes were deposited on TiO_2 nanotubes, enabling the directional transfer of photogenerated charge carriers and showing nearly full spectrum absorption with excellent photocatalytic activity for H_2 evolution.[123] Feng et al. described a binary $Mn_{0.2}Cd_{0.8}S$/Co_3O_4 transformed to ternary $Mn_{0.2}Cd_{0.8}S$/MoS_2/Co_3O_4. By producing a type-II heterojunction, the synergistic interaction of the $Mn_{0.2}Cd_{0.8}S$/Co_3O_4 p−n junction and MoS_2 enhance photocatalytic H_2 production. The few-layered MoS_2 served as a cocatalyst with a low CB position, providing electron transport from the CB of $Mn_{0.2}Cd_{0.8}S$ to the CB of MoS_2 and Co_3O_4, respectively.[124]

Systematic incorporation of the different constituents in a ternary composite was essential for increasing solar absorption and H_2 evolution reactions. Liu et al. constructed an Au-Cu nanoalloy/TiO_2/MoS_2 ternary composite by combining the Au-Cu nanoalloy and TiO_2/MoS_2 nanosheets. The high surface area of the TiO_2/MoS_2 hybrid improves sunlight absorption, and the Au-Cu nanoparticles serve as a bridge to connect the MoS_2 and TiO_2 via the surface plasmon resonance phenomenon.[125] Chen et al. synthesized a CdS/MoS_2/Mxenes ternary hybrid for the first time. When irradiated to visible light, the compound exhibits remarkable photocatalytic activity, with an H_2 production rate of 9679 μmol g^{-1} h^{-1}.[126] Another MoS_2/CQDs/$ZnIn_2S_4$ nanocomposites exhibit enhanced H_2 evolution activity with an apparent quantum efficiency of 25.6%.[127] The separation of photogenerated charge carriers and the resulting photocatalytic activity was

https://doi.org/10.1021/acsomega.3c02084
ACS Omega 2023, 8, 25649−25673

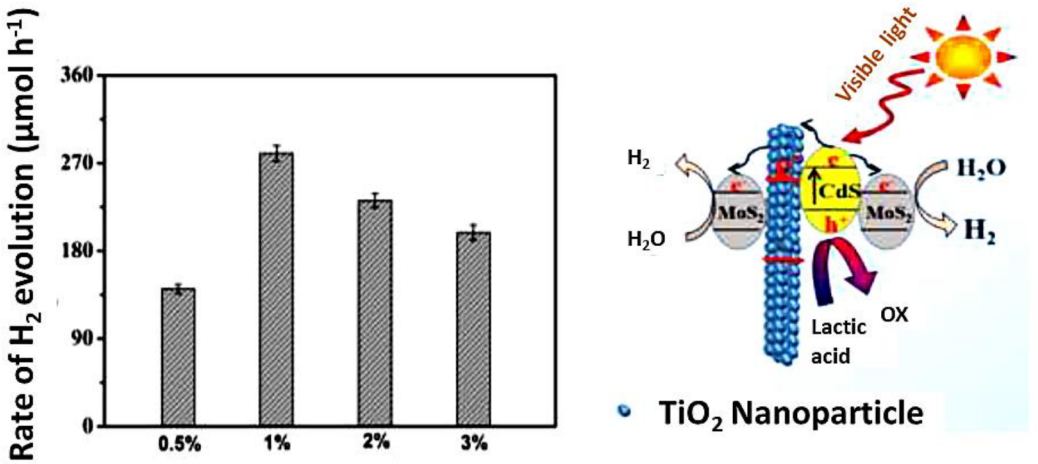

Figure 8. (Left) Photocatalytic H_2 evolution rate on MoS_2/CdS-TiO_2 nanofibers. (Right) Schematic representation of MoS_2/CdS-TiO_2 nanofibers for photocatalytic H_2 evolution in the presence of visible light irradiation ($\lambda \geq 420$ nm). Reproduced with permission from ref 132. Copyright 2017 Elsevier.

considerably enhanced by the fabrication of 0D/2D heterostructures. Guan et al. developed a $ZnIn_2S_4$/MoS_2-RGO nanosheets 0D/2D nanocomposite through a fast, low-temperature hydrothermal process. The MoS_2/RGO nanosheets support inhibiting 0D $ZnIn_2S_4$ nanoparticles from aggregation in the ternary heterostructure, resulting in a significantly higher H_2 generation than pure $ZnIn_2S_4$. The $ZnIn_2S_4$/MoS_2-RGO composite benefited from the superior visible light absorption characteristics of MoS_2 and RGO.[128] The sheetlike MoS_2/CdS/TiO_2 ternary structure exhibited exceptional stability and a high H_2 evolution rate of 4146 μmol g^{-1} h^{-1} under visible light. In this case, the conduction band of MoS_2 enhances the transfer of photoexcited electrons from sunlight on CdS to porous TiO_2 for photocatalytic H_2 generation. Conducting MoS_2 can increase the conductivity of the photocatalyst and reduce the photocorrosion of CdS as a hole collector.[129] Another ternary composite with similar results includes $CuInS_2$QDs/TiO_2/MoS_2 and gC_3N_4/red phosphorus/MoS_2. The H_2 evolution activity in these structures was 1034 μmol g^{-1} h^{-1} and 257.9 μmol g^{-1} h^{-1}, respectively.[130,131] The effective electrospinning and photodeposition process developed a unique ternary structure, MoS_2/CdS-TiO_2 nanofiber. The electro-spun TiO_2 nanofibers have the advantages of improved CdS and MoS_2 dispersion. The influence of MoS_2 deposition on H_2 production was investigated. When the concentration of MoS_2 increases from 0.5 to 1%, the H_2 evolution rate also increases. The photocatalytic performance for H_2 evolution in the 1% MoS_2/CdS-TiO_2 sample is significantly higher (280.0 μmol h^{-1}) than others (Figure 8a). The active hydrogen sites of MoS_2 can minimize the overpotential and enhance photocatalytic H_2 evolution. On the basis of the process (Figure 8b), photoexcited electrons can instantly be transported to the H_2 evolution active sites of MoS_2 and indirectly migrated to MoS_2 through TiO_2 as a bridge, enhancing the H_2 evolution rate. The unique structure of the heterojunction accomplished this and close intrafacial contact.[132] Ternary composites of CdS/MoS_2/MWCNTs composite photocatalyst were reported by Jo et al. The few-layered MoS_2 nanosheets exhibit high absorption and photoluminescence. A transient photocurrent density of 11.12 mA cm^2 illustrates the charge separation ability of the hybrid, confirming the transport of electrons from photoexcited CdS to MoS_2 edges along MWCNTs.[133] Similar results were obtained for the bifunctional ternary heterostructure In_2S_3/MoS_2/CdS composite.[134] The defect-rich MoS_2 in $Cd_{1-x}Zn_xS$/MoS_2/graphene hollow spheres performs as a low-cost cocatalyst to accelerate the photocatalytic H_2 evolution reaction. Few-layered MoS_2 having exposed active edges can take electrons directly from CdS or as an electron transfer medium via graphene. This heterostructure obtained an optimal H_2 production activity of 2.97 mmol h^{-1} g^{-1} (Table 2).[135] Furthermore, photocatalysts for HER over $ZnIn_2S_4$ were synthesized using MoS_2 nanosheets on the surface of hollow carbon spheres (C/MoS_2) and Co_3O_4 nanoparticles. The optimized C/MoS_2@$ZnIn_2S_4$/Co_3O_4 composite shows a photocatalytic H_2 evolution rate of 6.7 mmol g^{-1} h^{-1}. The enhanced photocatalytic activity is due to a dual photo generated process in which C/MoS_2 produces a Schottky heterojunction involving $ZnIn_2S_4$ and $ZnIn_2S_4$ which makes an S-scheme heterojunction with Co_2O_4. Additionally, the core−shell structure of the composite encourages intimate contact between constituents, enabling the separation of charge carriers.[136] Similar observations were reported in another $ZnIn_2S_4$ ternary structure containing hollow carbon spheres (HCSs) with MoS_2. The synergistic effect of MoS_2 and HCSs effectively facilitates H_2 production.[137] Ran et al. fabricated a microporous "S" doped NH_2-UiO-66 bridged $ZnIn_2S_4$/MoS_2 sheet structure (MS/ZIS) photocatalyst. The synthesized MS/ZIS photocatalyst exhibits a relatively high H_2 production rate of 5.69 mmol h^{-1} g^{-1}. The "S" doped NU66 creates a new electron transport path, which benefits electron transport to the surface and active edge sites of MoS_2.[138]

A two-step solvothermal approach followed by an in situ deposition technique was used to generate the oxygen-incorporated MoS_2 (O-MoS_2) coated on 1D $Cd_{1-x}Zn_xS$ with NiO_x ternary nanostructures. NiO_x nanoparticles were effectively grown on $Cd_{1-x}Zn_xS$@O-MoS_2 to construct unique $Cd_{1-x}Zn_xS$@O-MoS_2/NiO_x composites. By exchanging the S-sites, oxygen is integrated into the MoS_2 lattice. The longitudinal dimension of 1D CdZnS nanocrystals may serve as an effective channel. If the produced O-MoS_2 contains many structural defects, the photoexcited electrons in CdZnS and O-MoS_2 may also transfer to NiO_x, extending the recombination procedure considerably (Figure 9).[139] For photocatalytic H_2

https://doi.org/10.1021/acsomega.3c02084
ACS Omega 2023, 8, 25649−25673

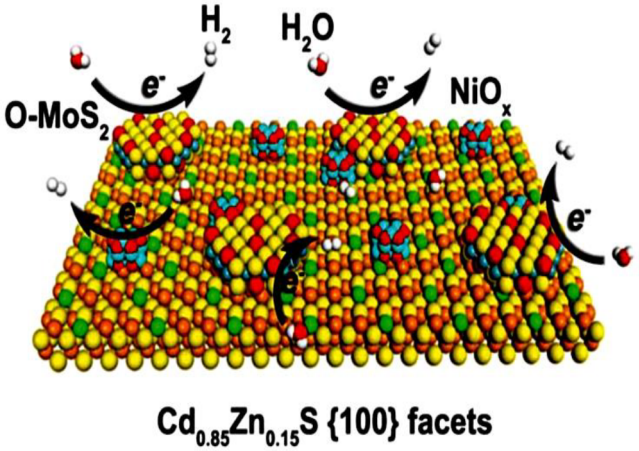

Figure 9. Schematic showing the photocatalytic HER over $CZ_{0.15}S$@ O-MoS_2/NiO*x*. Reproduced with permission from ref 139. Copyright 2019 Wiley.

production, a ternary heterostructure of $Ti_3C_2/MoS_2/CdS$ was produced. In this report, MoS_2 was formed in situ on Ti_3C_2 via electrostatic self-assembly, and hydrothermal techniques exhibited a vertically aligned framework suitable for more active edge sites for H_2 production. This binary structure served as a cocatalyst for H_2 evolution. It increases electron transport and prevents the recombination of electron−hole pairs formed from CdS by availing of the synergistic interactions of the MoS_2/Ti_3C_2 structures.[140]

Noble metals are generally recognized as excellent cocatalysts for photocatalytic H_2O splitting reactions. A substantial surface plasmon resonance (SPR) phenomenon can contribute to a greater absorption cross-section with higher energy density of trapped electrons, resulting in rapid H_2 production in photocatalytic splitting of water.[141,142] Ternary composites of MoS_2 containing noble metals have attracted much attention due to its high H_2 evolution activity. An Au nanoparticle deposited ternary Au-MoS_2/Ti_3C_2 photocatalyst was prepared using a hydrothermal method. The synthesized composite can modify electron transport paths. Due to the surface plasmon resonance effect of Au nanoparticles, the deposited Au nanoparticles on the surface of MoS_2 were excited, thereby improving the photocatalytic hydrogen evolution rate.[143] Similarly, the Pt-decorated ternary system, MoS_2/Pt-TiO_2, was efficiently developed by depositing MoS_2 nanosheets to Pt-TiO_2 frameworks. Appropriate ratios of MoS_2 and Pt inhibited the recombination of photogenerated charge carriers. The rate of H_2 evolution reaches 4.18 mmol h^{-1} g^{-1}, which is around 41.8 times higher than pure TiO_2. This unique method provides a path for transferring excited electrons from TiO_2 particles using MoS_2 and Pt nanoparticles as a link to facilitate proton reduction into H_2.[144] The sequential attachment of Au nanocrystals and CdS onto two-dimensional exfoliated MoS_2 nanosheets (e-MoS_2) was successfully fabricated by forming internally coupled plasmonic metal semiconductor hybrids. Due to their distinct band structure, the CdS and exfoliated MoS_2 will have a wide optical absorption range. Moreover, its 2D morphology allows e-MoS_2 to construct hybrids effectively with exposed surfaces.[145] Similar results were observed for the compound AgInZnS/MoS_2-GO, which exhibited the maximum hydrogen evolution activity of 1302 μmol h^{-1}. The higher H_2 evolution activity of the composite arises due to the synergetic effect of graphene and MoS_2, where graphene facilitates the charge transfer, and MoS_2 provides more active sites for H_2 evolution.[146] The Au nanoparticle-incorporated ternary CdS-Au/MoS_2 core−shell hollow structure demonstrated the strongest visible-light photocatalytic H_2 evolution. Electron and hole recombination was efficiently reduced after the formation of heterostructures by CdS, MoS_2 nanosheets, and Au NPs, resulting in increased H_2 generation. Figure 10 illustrates the reaction pathway for

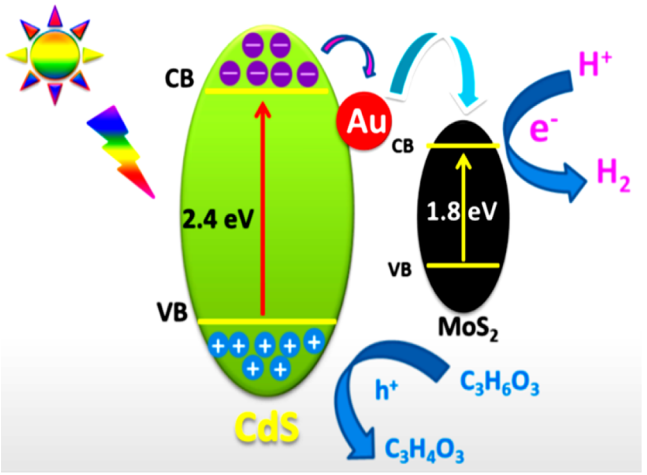

Figure 10. Schematic illustration for the charge separation and enhanced H_2 evolution activity in CdS-Au/MoS_2 composites. Reproduced from ref 147. Copyright 2018 American Chemical Society

H_2 evolution. The SPR effects of Au NPs stimulate photon absorption and accelerate electron transport, acting as an electron mediator from CdS to MoS_2. During visible light excitation, the electrons produced by CdS are transported into the CB of MoS_2 nanosheets via the Au NPs. MoS_2 nanosheets are electronic sinks and provide active sites for the photocatalytic H_2 evolution reaction.[147]

In another study, AuNPs@MoS_2/ZnO nanorod hybrid structure has been successfully synthesized and shows excellent stability for H_2 production. The MoS_2 seemed like a monodispersed sphere with a diameter of ∼400 nm and composed of tangled MoS_2 nanosheets. Introducing Au NPs into MoS_2 microspheres results in a core−shell hybrid with improved plasmonic absorption. Adding ZnO nanorods into this system further enhances optical absorption. Mutual interactions between Au NPs (or ZnO nanorods) and MoS_2 spheres efficiently prevent MoS_2 nanosheets from peeling off from the spheres. Thus, after a 32 h test, the hybrid exhibited promising H_2 production activity of 13.56 μmol g^{-1} min^{-1} with increased stability of 91.9%. This is one of the highest photocatalytic activities among the MoS_2-based photocatalysts.[148] Table 3 summarizes the different MoS_2/noble metal composites, the synthesis method, and the photocatalytic parameters for producing H_2 from the photocatalytic water splitting.

3. PHOTOCATALYTIC CARBON DIOXIDE REDUCTION REACTION (PCO_2RR)

Carbon dioxide (CO_2), the most abundant greenhouse gas, contributed significantly to global warming. Different techniques have been developed to decrease the amount of CO_2 in the atmosphere, including absorption, bioconversion, and

https://doi.org/10.1021/acsomega.3c02084
ACS Omega 2023, 8, 25649−25673

Table 3. Summarized List of Photocatalytic Hydrogen Evolution of Ternary Composites of MoS_2

photocatalyst	synthesis method	light source	amount of catalyst	sacrificial reagent	H_2 evolution activity	ref
$CeO_2/MoS_2/g\text{-}C_3N_4$	hydrothermal	3 W UV LEDs	50 mg	80 mL aqueous solution containing 0.5 M Na_2SO_3 and 0.5 M Na_2S	65.4 μmol h^{-1}	114
$CoMoS_2/rGO/C_3N_4$	solvothermal	300 W Xe lamp	100 mg	mixed solution of TEOA and H_2O (volume ratio equal to 1/5)	684 μmol g^{-1} h^{-1}	115
ZnO/MoS_2/RGO	hydrothermal	natural sunlight	5.0 mg	45 mL aqueous solution contains 0.1 M Na_2S and 0.1 M Na_2SO_3	28.61 mmol g^{-1} h^{-1}	116
$CdS/WS_2/MoS_2$	hydrothermal	150 W Xe lamp	1.0 mg	20 vol % lactic acid	209.79 mmol g^{-1} h^{-1}	117
$CdS/Ni_2P/MoS_2$	hydrothermal	150 W Xe lamp	1.0 mg	15 mL aqueous solution containing 3 mL lactic acid	72.76 mmol g^{-1} h^{-1}	118
CdS/MoS_2/graphene	hydrothermal	300 W Xe lamp	30 mg	45 mL aqueous solution + 5 mL lactic acid	1913 μmol g^{-1} h^{-1}	119
$MoO_2/MoS_2/TiO_2$	CVD	300 W Xe lamp	–	100 mL aqueous solution contains 0.5 M ethylene glycol and 0.5 M Na_2SO_4	110 μmol h^{-1} cm^{-2}	123
$Mn_{0.2}Cd_{0.8}S/MoS_2/CoO_4$	solvothermal	300 W Xe lamp	0.05 g	100 mL aqueous solution contains 0.5 mol L^{-1} Na_2S and 0.5 mol L^{-1} Na_2SO_3	16.45 mmol g^{-1} h^{-1}	124
Au-Cu nanoalloy-TiO_2/MoS_2	hydrothermal and annealing	300 W Xe lamp	5 mg	aqueous solution contains 0.35 M Na_2S and 0.25 M Na_2SO_3	0.75 mmol g^{-1} h^{-1}	125
MXene/CdS/MoS_2	hydrothermal	300 W Xe lamp	5 mg	50 mL aqueous solution contains 0.25 M Na_2S and 0.35 M Na_2SO_3	9679 μmol g^{-1} h^{-1}	126
$ZnIn_2S_4$/CQDs/MoS_2	hydrothermal	300 W Xe lamp	50 mg	100 mL aqueous solution contains 10 mL TEOA	133 μmol h^{-1}	127
$ZnIn_2S_4/MoS_2$/RGO	hydrothermal	300 W Xe lamp	50 mg	100 mL 20% v/v lactic acid solution	425.1 μmol g^{-1} h^{-1}	128
$CuInS_2$ QDs/TiO_2/MoS_2	ultrasonic dispersion and annealing	300 W Xe lamp	50 mg	250 mL aqueous solution contains 0.1 M Na_2S and 0.1 M Na_2SO_3	1034 μmol g^{-1} h^{-1}	130
$g\text{-}C_3N_4$/red phosphorus/MoS_2	in situ photodeposition	300 W Xe lamp	10 mg	9 mL aqueous solution contains 1 mL TEOA	257.9 μmol g^{-1} h^{-1}	131
$CdS/TiO_2/MoS_2$	electrospinning andphotodeposition	300 W Xe lamp	20 mg	80 mL aqueous solution contains 10 vol % lactic acid	280 μmol h^{-1}	132
CdS/MoS_2/MWCNTs	hydrothermal	300 W Xe lamp	20 mg	45 mL H_2O + 5 mL lactic acid	676.0 μmol g^{-1} h^{-1}	133
$Cd_{0.8}Zn_{0.2}S/MoS_2$/graphene	hydrothermal	300 W Xe lamp	50 mg	96 mL H_2O + 4 mL lactic acid	2.97 mmol g^{-1} h^{-1}	135
NH_2-UiO-66 bridged $ZnIn_2S_4/MoS_2$	hydrothermal	300 W Xe lamp	40 mg	80 mL aqueous solution contains 10% TEOA	5.69 mmol g^{-1} h^{-1}	138
$Cd_{1-x}Zn_xS$@$OMoS_2/NiO_x$	hydrothermal	300 W Xe lamp	10 mg	100 mL aqueous solution contains 0.35 M Na_2S and 0.25 M Na_2SO_3	66.08 mmol g^{-1} h^{-1}	139
Au-MoS_2/Ti_3C_2	hydrothermal	300 W Xe lamp	30 mg	50 mL methanol solution (deionized H_2O: 70%, methanol: 30%)	12000 μmol g^{-1} h^{-1}	143
Pt-TiO_2/MoS_2	hydrothermal	300 W Xe lamp	20 mg	100 mL solution contains 0.25 M Na_2S and 0.5 M Na_2SO_3	4.18 mmol g^{-1} h^{-1}	144
CdS-Au/MoS_2	hydrothermal	300 W Xe lamp	10 mg	50 mL aqueous solution contains 10% lactic acid	237.90 μmol g^{-1} h^{-1}	147
Au-ZnO/MoS_2	hydrothermal	300 W Xe lamp	0.05 g	50 mL deionized H_2O contains 0.3 M Na_2S and 0.3 M Na_2SO_3	13.56 μmol g^{-1} min^{-1}	148

photocatalytic reduction.[149−151] Compared to photocatalytic H_2 evolution, CO_2 reduction by photocatalysis is a more complicated and challenging photochemical process. The products of photocatalytic CO_2 reduction are selective and depend on several conditions. To address the significant issues of the preliminary modification processes, it must tackle both the challenges of thermodynamic and kinetic factors. Being a stable linear molecule, CO_2 has a high bond energy of 750 kJ mol^{-1}. The thermodynamic aspect of photocatalytic CO_2 reduction requires an efficient light-responsive semiconductor that can capture enough external energy to break the C═O bond, essential for producing the C−H bond and synthesizing hydrocarbons.[152,153] The interactions of intermediates with the surface of the catalyst determine product selectivity in CO_2 reduction. Therefore, to attain maximum output during photocatalytic CO_2 reduction, the photocatalyst should first satisfy the fundamental criteria: interact with the substrate molecules to start the transition process on the catalyst's surface (CO_2 or H_2O). Another governing factor is photon absorption for exciting electrons from the catalyst's valence band (VB) to the conduction band (CB). After excitation, the higher energy electrons in the CB showed higher potentials for CO_2 reduction. As a result, catalysts with suitable band gaps (1.4−3 eV) are necessary to attain the maximum CO_2 reduction.[154,155] Since the first report by Inoue and co-workers on the photocatalytic reduction of CO_2 to formaldehyde and methanol,[156] various photocatalytic materials have been developed for photocatalytic CO_2 reduction, including metal oxides,[157,158] sulfides,[159] perovskite-like materials,[160] double-layered hydroxides,[161] and layered materials.[162,163] Among them, the transition metal dichalcogenides (TMD) find their application for CO_2 transformation through electrocatalytic, thermochemical, and photocatalytic ways. Even though photocatalytic H_2 evolution using TMD is well-known, their use in photocatalytic CO_2 reduction has been recently reported. Mainly, photocatalytic CO_2 reduction using MoS_2 is an emerging area that is considered a future photocatalyst for CO_2 reduction and a favorable, cost-effective alternative for

https://doi.org/10.1021/acsomega.3c02084
ACS Omega 2023, 8, 25649−25673

noble metal catalysts, exhibiting remarkable CO_2 electrochemical reduction activity with a high current density and low overpotential. The 2D layered nanostructures enable the modification and tunability of other TMDs. The atomic thickness allows for excellent optical transparency and mechanical flexibility, possibly allowing more surface-active sites over MoS_2. The small diffusion path length and presence of terminated edges of MoS_2 act as an active center for the CO_2 reduction reaction, facilitating multiple electron transfers.[164−166]

Interestingly, MoS_2-based catalysts exhibit superior electrochemical selectivity over alcohols than other catalysts. In particular, alcohol synthesis from syngas has also been evaluated.[167,168] Asadi et al. in 2014 reported that a layer-stacked bulk MoS_2 containing molybdenum (Mo)-terminated edges showed superior CO_2 reduction activity. The metallic nature of MoS_2, the large d-electron density, and the availability of molybdenum-terminated edges are the primary reasons for the catalytic activity, which facilitates multiple electron transfer processes in the CO_2 reduction pathway.[169] Recently, researchers have focused on photocatalytic CO_2 reduction using MoS_2-based photocatalysts. Xie et al., for example, showed that the catalytic process over MoS_2 proceeds via a carboxylate pathway, viz., $CO_2 \rightarrow COOH^* \rightarrow CO^* \rightarrow CO$ to produce CO as the final product.

Due to the low energy barrier of CO, the method suggests more excellent selectivity toward CO than other products like HCOOH and CH_3OH. Theoretical calculations indicate that the center of the d band at Mo exposed atoms at the edges is much closer than the metallic catalysts (e.g., Pt); thus, close interactions occurred with the adsorbed species. Meanwhile, the partial density of states (PDOS) of the activated CO_2* and the exposed Mo atoms shows the strong interactions of Mo and O compared to the Mo−C interactions, which initiates the cleavage of the C═O bond to activate CO_2*. The exposed edges are responsible for adsorbing the CO_2 molecule and activating the two neighboring Mo atoms. The first transfer of e^- or h^+ across the MoS_2 edges is thought to be a hydrogenation step that controls the reduction pathway. It forms the unstable intermediate HO-CO*, which quickly decomposes to OH* and CO*. The hydrogenation of COOH* controls the product selectivity for CO and other hydrocarbons.[170] Due to the low band gap potential, the charge recombination occurring over the surface of MoS_2 is becoming a significant challenge. Forming products like CH_3OH and CH_4 is also difficult because this involves 6 e^- and 8 e^- processes, respectively, compared to products like CO, which require only two e^- that can be directly used as fuels and transformed into other powers through energy-intensive processes.[171] Therefore, effective doping and heterojunction formations are required to get a more significant number of electrons available for reducing CO_2, thereby increasing the efficiency of the MoS_2-based photocatalysts for CO_2 reduction. The remaining sections will focus on the roles of MoS_2 and the various transformations that occurred as a transpire photocatalyst in CO_2 reduction reactions.

3.1. MoS_2 Nanostructures for Photocatalytic CO_2 Reduction. The MoS_2 nanoflower-like morphology with dangling bonds at the stacked sheet edge makes it ideal for photocatalytic CO_2 reduction. Meier et al. reported a controllable edge-rich nanoflower morphology with abundant edge sites through a chemical vapor deposition (CVD) method. Photocatalytic activity increases with increasing edge plane density of nanoflower due to unsaturated and dangling bonds. During CVD synthesis, the energy gap (Eg) was separately varied from 1.38 to 1.83 eV. Carbon monoxide (CO) was the most prominent product of CO_2 photoreduction in the presence of H_2O. The production rates of CO nearly doubled after a post-treatment reduction step. This reliable CVD technique contributes to developing efficient and stable 2D-MoS_2 nanoflower materials for CO_2 reduction.[172] MoS_2 nanosheets combined with metal oxides were identified as a cost-effective substitute for noble metal cocatalyst for photocatalytic reduction of CO_2. Tu et al. reported the formation of a 2D-MoS_2 nanosheet on TiO_2 nanosheets. To reduce CO_2 by UV−vis light irradiation, pure TiO_2 nanosheets and MoS_2/TiO_2 hybrid nanosheets were placed in a CO_2-saturated 1 M $NaHCO_3$ aqueous solution. The CH_3OH production of 0.5 wt % MoS_2/TiO_2 reached to 10.6 μmol g^{-1} h^{-1}, which was 2.9 times that of pure TiO_2 (3.7 μmol g^{-1} h^{-1}). The fast electron transport from TiO_2 to MoS_2 is indicated by the PL decay lifetime of 0.51 ns. The weak van der Waals interactions in the S−Mo−S layers result in Mo-terminated edges containing high d-electron density, which contributes to excellent and selective photocatalytic CO_2 reduction.[173] Similarly, few-layered MoS_2 with uniformly formed mesoporous TiO_2 on the surface of 3D graphene showed higher photocatalytic CO_2 reduction. The MoS_2 layers in the 3D aerogel perform as a cocatalyst to minimize the backward charge transfer through graphene to TiO_2. The few-layered MoS_2 with unsaturated S atoms on exposed edges improved its activity and generated a high electron concentration in the composite between the MoS_2 and graphene layers. The yield of CO formation was up to 92.33 μmol g^{-1} h^{-1}.[174]

Jia et al. recently synthesized a MoS_2/TiO_2 heterojunction photocatalyst for CO_2 reduction. The ultrathin MoS_2 nanosheets were equally combined with the TiO_2 nanoparticles. The conduction band (CB) edge potential of MoS_2 (−0.93 V) was more negative than that of TiO_2 (−0.55 V), so the photogenerated electrons on the surface of MoS_2 sheets could easily migrate to TiO_2. CO and CH_4 were the major products in the experimental process, and the 10% MoS_2/TiO_2 composite gave the maximum yield. It is about 268.97 μmol g^{-1} and 49.93 μmol g^{-1}, respectively.[175] Xu et al. constructed a 1D/2D TiO_2/MoS_2 nanostructure composite. Here, the MoS_2 sheet arrays with lateral dimensions of 80 nm with thicknesses of up to 2 nm were firmly connected to the surface of TiO_2 nanofiber. The CO_2 adsorption and surface area of the produced samples increase as the MoS_2 loading increases. With increasing CO_2 loading, the CH_4 and CH_3OH synthesis rates increase, reaching a maximum of 2.86 and 2.55 μmol g^{-1} h^{-1}, respectively, with a quantum yield of 0.16% for the best TiO_2/MoS_2 sample (TM10). The DFT calculations further demonstrate that MoS_2 has a higher work function than TiO_2, resulting in electron transfer from MoS_2 to TiO_2 upon photoexcitation.[176]

A type II p-n heterojunction charge transfer model was formed by coupling the α-Fe_2O_3 and MoS_2 composite. The loading of α-Fe_2O_3 promoted 2H to 1T MoS_2 phase conversion and increased charge carrier migration. In situ diffuse reflectance infrared Fourier transform spectroscopy (DRIFTS) analysis revealed a deoxygenation pathway for CO_2 conversion. Several intermediate species are formed upon the adsorption of CO_2, which ultimately results from excellent CO_2 reduction performance to CH_4 and CH_3OH.[177] In

https://doi.org/10.1021/acsomega.3c02084
ACS Omega 2023, 8, 25649−25673

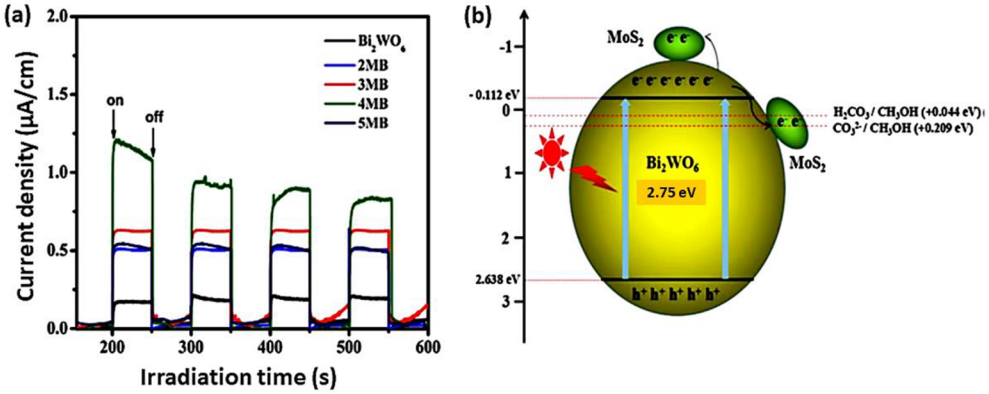

Figure 11. (a) Transient photocurrent response of Bi_2WO_6 and MoS_2/Bi_2WO_6 nanocomposites under visible light irradiation. (b) Proposed CO_2 photoreduction and charge transfer mechanism in the MoS_2/Bi_2WO_6 nanocomposite. Reproduced with permission from ref 178. Copyright 2017 Elsevier.

another system, a few-layered MoS_2-loaded flowerlike Bi_2WO_6 nanocomposite was reported by Dai et al.[178] The as-prepared composites showed an excellent photoreduction of CO_2 into hydrocarbons compared to pure Bi_2WO_6. The intimate interfacial contact between MoS_2 and Bi_2WO_6 significantly influenced the transfer of photogenerated charge carriers. The composite also showed much stronger absorption within the visible region than pure Bi_2WO_6. The photocurrent response of the composites (Figure 11a) provided information about the higher separation efficiency of photogenerated charge carriers. The methanol and ethanol obtained from the optimized sample (0.4 wt % MoS_2) after 4 h of visible light irradiation were 36.7 and 36.6 μmol g^{-1}, respectively, 1.94 times higher than pure Bi_2WO_6.

A possible photocatalytic mechanism (Figure 11b) was also proposed. It indicated that the CO_3^{2-}, HCO_3^-, and H_2CO_3 formed in the aqueous solutions might serve as reactive carbon sources during the photoreduction process. The 2D-π conjugated structure could serve as an electron-accepting material and contribute to separating e^--h^+ pairs for CO_2 reduction.[178] A flowerlike $MoS_2/Ag/SnO_2$ ternary composite that serves as a bifunctional catalyst for photocatalytic CO_2 reduction and degradation of pollutants was recently produced using a simple hydrothermal process. Because of the high specific surface area, several folded edges, and ultrathin nature, Ag nanoparticles and SnO_2 NSs were distributed uniformly on the MoS_2 surface, enhancing photoexcited charge transport. The modified $MoS_2/Ag/SnO_2$ nanocomposites exhibit outstanding visible-light photocatalytic activity for converting CO_2 to methane (CH_4). The quantum efficiency calculated at λ = 420 nm was found to be 2.38% which substantiates the high CO_2 conversion efficiency of the catalyst. SnO_2 accepts the photogenerated electron of MoS_2 through Ag in the heterojunction, which directly reduces CO_2 and produces CH_4 as the final product. Besides CO_2 reduction, the composite also shows high activities for pollutant degradation.[179] Another binary composite using 2D MoS_2 nanosheets with a metal sulfide has been reported. The p-n heterostructure Bi_2S_3-MoS_2 nanocomposite revealed improved sunlight absorbance and photocatalytic reduction of CO_2. The high catalytic performance was due to the increased S-defects on the MoS_2 surface, hence increasing interfacial interaction between MoS_2 and Bi_2S_3.[180] As mentioned in the first section, graphitic carbon nitride (gC_3N_4) can be an efficient photocatalyst to construct the heterojunction with layered MoS_2. Studies have been reported regarding the applications of MoS_2/g-C_3N_4 nanocomposites for photocatalytic reactions to convert CO_2 to hydrocarbons. Recently, Qin et al. mentioned the synthesis of MoS_2/gC_3N_4 nanocomposites to convert CO_2 into fuels by a simple hydrothermal followed by a calcination process. The synthesized 10% MoS_2/g-C_3N_4 heterojunction exhibited the highest conversion efficiency in reducing CO_2 to CO up to 58.59 μmol g^{-1} and showed significant stability after a seven-hour reaction. Z-Scheme charge transfer was constructed by correctly coupling the two semiconductor photocatalysts for CO_2 reduction.[181]

Combining semiconductors with noble metal NPs (Ag, Au, or Pt) caused localized surface plasmon resonance (LSPR) to show great potential in photocatalytic CO_2 reactions. Interestingly, studies have confirmed that the generation of LSPR can optimize the structure of MoS_2. Sun et al. demonstrated the Au nanoparticle decorated ultrathin MoS_2 nanosheet acts as an excellent heterogeneous catalyst for photocatalytic CO_2 reduction. The DFT calculations also endorse the experimental data. DRIFTS spectrum proposed a reaction pathway for the formation of CH_4, $CO_2 \rightarrow COO- \rightarrow -COOH \rightarrow -HCO \rightarrow -HCOH \rightarrow -CH_2OH \rightarrow -CH_3 \rightarrow CH_4$ via the hydrogenation process. For the Au-MoS_2 sample, the reaction barrier for forming a COOH intermediate decreases from 2.17 to 1.82 eV, suggesting faster CO_2 reduction.[182] Similarly, a DFT study on Ag-loaded 2H-MoS_2 was stimulated by Ouyang et al. for the photocatalytic reduction of CO_2. From the series of Ag loading on the 2H-MoS_2 nanosheet, the 20 wt % Ag/MoS_2 is most suitable for converting CO_2 to CH_4. The Gibbs free energy was reduced from 2.830 to 0.925 eV for the 20 wt % Ag/2H-MoS_2 nanocomposite.[183]

For adjusting the band gap of MoS_2, phase conversion via chemical exfoliation was used. In a recent study, Zheng et al. reported the synthesis of Ag/2H-MoS_2 composites and their photocatalytic activity in reducing CO_2 to methanol. A wet chemical process was invented to exfoliate MoS_2 nanosheets and transform them from the 1T phase to the 2H phase. This composite obtained a larger specific surface area through Li-ion intercalation and exfoliation than the hydrothermally synthesized MoS_2. The Ag nanoparticles can act as a pool for collecting the photogenerated electrons of MoS_2 nanosheets and suppress the recombination of charge carriers. The maximum yield of methanol obtained after 10 h irradiation at 20 wt % Ag/2H-MoS_2 was about 365.08 μmol g^{-1} h^{-1}.[184] A

https://doi.org/10.1021/acsomega.3c02084
ACS Omega 2023, 8, 25649−25673

study by Lu et al. demonstrated the use of a noble metal-free catalyst ($Mn_{0.2}Cd_{0.8}S$) wrapped in a series of MoS_2 ultrathin nanosheets for photocatalytic energy conversion. The optimal loading of MoS_2 content was 3%, giving an H_2 production rate of 335.02 μmol h^{-1} and a CH_3OH production rate of 2.13 μmol h^{-1}. The production of methanol increases with increasing the MoS_2 content. The improved photocatalytic efficiency benefits from the intimate interfacial contact between $Mn_{0.2}Cd_{0.8}S$ and MoS_2, which effectively promotes the separation and transportation of photogenerated charge carriers.[185]

Recently, a composite comprising MoS_2 and a halide perovskite material, $CsPbBr_3$, formed a stable heterojunction. The heterojunction contacts between the two components increased the lifetime confirmed by the PL, surface, and transient photovoltage (SPV, TPV) and DFT studies. The temperature-programmed CO_2 desorption (TPD) analyses showed that introducing MoS_2 increased the ability of the CO_2 uptake of the composite.[186] CO_2 photoreduction and simultaneous H_2 production were achieved by a ternary nanocomposite of MoS_2 and N-containing polymer polypyrrole (PPy) on reduced graphene oxide (rGO). The resulting rGO-MoS_2/PPy nanocomposites reveal that rGO-MoS_2 acts as a rigid template, ensuring consistent growth and heterogeneous nucleation of PPY, thereby increasing their photocatalytic reduction of CO_2 into CH_4, CO, and H_2. Composites containing optimal amounts of PPy (rGO-MoS_2/PPy-150) exhibited the highest photocatalytic activity to CO (3.95 μmol g^{-1} h^{-1}), CH_4 (1.50 μmol g^{-1} h^{-1}), and H_2 (4.19 μmol g^{-1} h^{-1}), with a quantum yield of 0.30%.[187] Similarly, a simple solvothermal method constructed a novel S−C−S heterojunction by Yin et al. The MoS_2 was assembled into 3D-uniform nanoflower balls after a simultaneous coupling connection with rGO and SnS_2. The valence band (VB) positions of pure MoS_2 (1.61 eV) and SnS_2 (1.50 eV) indicate that they can form an effective Z-type heterojunction so that the electrons can quickly be excited from the MoS_2 CB to VB in SnS_2 and thereby to rGO to reduce CO_2 to CO and CH_4.

The multilevel electron transport produces CO and CH_4 up to 68.53 and 50.55 μmol g^{-1} h^{-1}, respectively.[188] A binary photocatalyst composed of the SiC@MoS_2 nanoflower was reported by Wang et al. for simultaneous photocatalytic CO_2 reduction and H_2O oxidation under visible light. All the SiC@MoS_2 samples show much higher CH_4 evolution than the individual components. The optimized samples show the CH_4 evolution up to 323 μL g^{-1} h^{-1} and O_2 evolution of about 620 μL g^{-1} h^{-1} with high photocatalyst stability. The photocatalytic reduction of CO_2 follows the hydrogenation pathway (Figure 12). One CO_2 molecule is converted into one CH_4 by four sequential hydrogenation half-cell reactions. This pathway takes advantage of the photoreduction potential of SiC and the powerful photoreduction ability of MoS_2 nanosheets.[189]

Layered double hydroxides (LDH) are a new materials class that has recently attracted much interest. A study by Zhao et al. demonstrated that the heterojunction of MoS_2 with Co-Al-LDH through an electrostatic interaction facilitates the charge transfer and syngas production by controlling the heterojunction concentration. Photogenerated electrons spontaneously transfer from LDH CB to MoS_2, and the syngas ratio (H_2:CO) was precisely turned from 1.3:1 to 15:1 by altering only the catalyst concentration in the photocatalytic CO_2 reduction under visible light.[190]

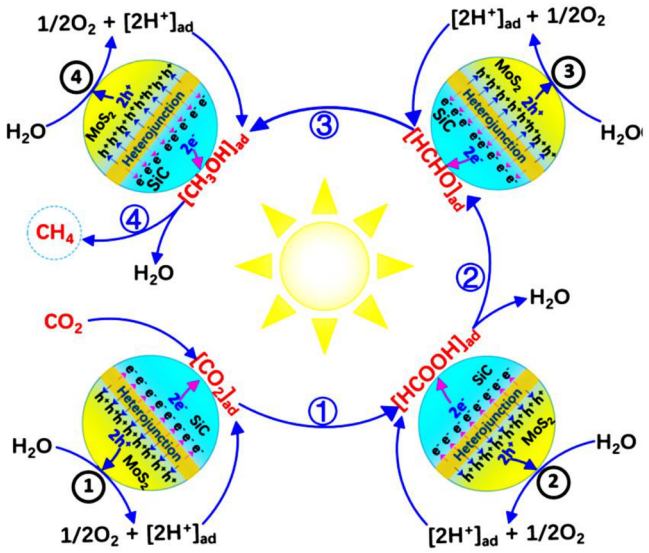

Figure 12. Reaction pathway for photocatalytic CO_2 reduction by H_2O on SiC@MoS_2. Reproduced from ref 189. Copyright 2018 American Chemical Society.

A multidimensional ternary heterojunction of Bi_2S_3/TiO_2/MoS_2 was reported by Alkanad et al. for the photocatalytic CO_2 reduction reaction where Bi_2S_3 and TiO_2 were embedded and wrapped within the MoS_2 nanosheet. The in situ irradiated photoelectron spectroscopy (ISI-XPS) reveals the switchable feature of the heterostructure. Electron flow follows the S-scheme approach in UV−vis-NIR (CH_3OH and C_2H_5OH as the major products), whereas, in vis-NIR, it forms a type II heterojunction (CH_4 and CO), thus exhibiting a selective photocatalytic CO_2 reduction reaction. Moreover, the quantum efficiency of the system reaches 4.23% at 600 nm wavelength.[191] Another higher CO_2 reduction capacity was observed in a ZnO/MoS_2 nanosheet composite where the hollow structure of MoS_2 encapsulates the ZnO nanoparticles and enables multiple refractions of photons in the cell. MoS_2 as a 2D sheet would enhance electron mobility, so the photogenerated electrons and holes are accumulated on the surface of MoS_2. Therefore, CB and VB of MoS_2 simultaneously reduce CO_2 and oxidize H_2O.[192] Metallic or nonmetallic doping creates defects in the MoS_2 lattice and facilitates charge transfer at the interface to facilitate CO_2 reduction. Such a ternary system in which In_2S_3 was decorated with MoO_3@MoS_2 was fabricated for visible light photoreduction of CO_2 to CH_4 and CO. The presence of In_2S_4 induces S-rich sites and O vacancies in the composite for CO_2 reduction, and a maximum yield of CH_4 (29.4 μmol g^{-1} h^{-1}) and CO (35.6 μmol g^{-1} h^{-1}) was obtained.[193] Similarly, duel In_2S_4-NiS decorated MoO_3@MoS_2 was reported by Zheng et al. through an in situ sulfurized approach of nonthermal plasma. Increasing the In_2S_4-NiS content into the MoO_3@MoS_2 system increased the CH_4 yield of 49.11 μmol g^{-1} h^{-1}.[194] Metal−organic frameworks (MOFs) were an excellent platform for developing heterogeneous catalysts for CO_2 reduction. By integrating MoS_2 nanosheets into hierarchically porous defective UiO-66 (d-UiO-66), a composite of d-UiO-66/MoS_2 was prepared for the selective photocatalytic reduction of CO_2 to CH_3COOH. The unsaturated Mo atoms on the MoS_2 nanosheet would contact d-UiO-66 to form Mo−O−Zr bimetallic sites for selective CO_2 reduction.

https://doi.org/10.1021/acsomega.3c02084
ACS Omega 2023, 8, 25649−25673

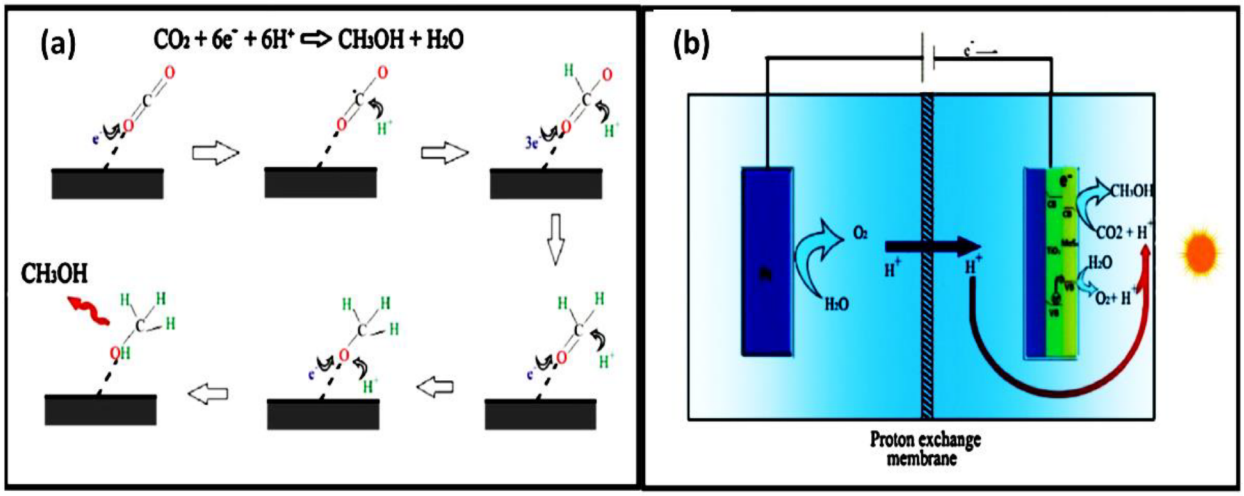

Figure 13. (a) Probable speculation reaction pathway for the reduction of CO_2 to CH_3OH. (b) Mechanism of the PEEC reducing CO_2 process at MoS_2-rods/TiO_2NTs electrode. Reproduced with permission from ref 198. Copyright 2014 Elsevier.

Table 4. Summarized List of Phototocatalytic Carbon Dioxide Reduction Using MoS_2 Compounds

photocatalyst	synthesis method	light source	amount of catalyst	major products	ref
MoS_2 nanoflower	CVD	solar simulator	150 mg	CO	172
MoS_2/TiO_2	hydrothermal	300 W Xe lamp	0.1 g	CH_4 (10.6 μmol g^{-1} h^{-1})	173
TiO_2/MoS_2/graphene	hydrothermal	300 W Xe lamp	–	CO (92.33 μmol g^{-1} h^{-1})	174
MoS_2/TiO_2	hydrothermal	300 W Xe lamp	50 mg	CO (268.97 μmol g^{-1}) CH_4 (49.93 μmol g^{-1})	175
TiO_2/MoS_2	hydrothermal	350 W Xe lamp	50 mg	CH_4 (2.86 μmol g^{-1} h^{-1}) CH_3OH (2.55 μmol g^{-1} h^{-1})	176
α-Fe_2O_3/MoS_2	hydrothermal	300 W Xe lamp	50 mg	CH_4 (121 μmol g^{-1} h^{-1}) CH_3OH (41 μmol g^{-1} h^{-1})	177
MoS_2/Bi_2WO_6	hydrothermal	300 W Xe lamp	50 mg	CH_3OH (36.7 μmol g^{-1}) C_2H_5OH (36.6 μmol g^{-1})	178
$SnO_2/Ag/MoS_2$	hydrothermal	300 W Xe lamp	–	CH_4 (20 μmol) CO (9 μmol)	179
Bi_2S_3/MoS_2	hydrothermal	150 mW cm^{-2} Xe lamp	0.2 g	CO (40 μmol g^{-1}) CH_4 (2.5 μmol g^{-1})	180
MoS_2/g-C_3N_4	hydrothermal	300 W Xe lamp	50 mg	CO (58.59 μmol g^{-1})	181
Au/MoS_2	hydrothermal and ultrasonic dispersion	300 W Xe lamp	0.025 g	CH_4 (19.38 μmol g^{-1} h^{-1})	182
Ag/MoS_2	hydrothermal, calcination and reduction	200 W Hg lamp	20 mg	CH_3OH (365.08 μmol g^{-1} h^{-1})	184
$MoS_2/Mn_{0.2}Cd_{0.8}S$	hydrothermal	300 W Xe lamp	50 mg	CH_3OH (2.13 μmol h^{-1})	185
polypyrrole/rGO/MoS_2	hydrothermal and ultrasonication	300 W Xe lamp	50 mg	CO (3.95 μmol g^{-1} h^{-1}) CH_4 (1.50 μmol g^{-1} h^{-1})	187
MoS_2/SnS_2/rGO	solvothermal	8 W Hg lamp	20 mg	CO (68.53 μmol g^{-1} h^{-1}) CH_4 (50.55 μmol g^{-1} h^{-1})	188
SiC/MoS_2	self-assembly	300 W Xe lamp	10 mg	CH_4 (323 μL g^{-1} h^{-1})	189
$Bi_2S_3/TiO_2/MoS_2$	microwave synthesis	300 W Xe lamp	50 mg	CH_3OH (119 μmol g^{-1}) C_2H_5OH (102.7 μmol g^{-1})	191
MoS_2@ZnO	calcination	150 W Hg lamp	0.1 g	CH_3OH (170.5 μmol g^{-1})	192
In_2S_3/MoO_3@MoS_2	in situ sulfurization	200 mW cm^{-2} Xe lamp	10 mg	CH_4 (29.4 μmol g^{-1} h^{-1}) CO (35.6 μmol g^{-1} h^{-1})	193
In_2S_3/NiS/MoO_3@MoS_2	in situ sulfurization	300 W Xe lamp	10 mg	CH_4 (49.11 μmol g^{-1} h^{-1}) CO (6.19 μmol g^{-1} h^{-1})	194
$ZnO/In_2O_3/MoS_2$	hydrothermal and ultrasonication	300 W Hg lamp	100 mg	CO (5.628 μmol g^{-1} h^{-1}) CH_4 (3.048 μmol g^{-1} h^{-1})	196

By loading the composite on a nylon 66 microfiltration membrane, CH_3COOH was formed with a rate of 39.0 μmol g^{-1} h^{-1} without any sacrificial reagent.[195] Similarly, a new In_2O_3/MoS_2 comodified ZnO nanorods also showed CO_2 photoreduction to CO and CH_4. Surface modification of the In_2O_3 and MoS_2 species would create transfer channels for holes and electrons on the photocatalyst's surface and improve the photocatalytic activity.[196]

3.2. MoS_2-Based Photoelectrocatalytic CO_2 Reduction. Cu_2O is a promising low-cost photocatalyst for CO_2

https://doi.org/10.1021/acsomega.3c02084
ACS Omega 2023, 8, 25649−25673

reduction, which showed higher selectivity for methanol formation. But their poor conductivity and charge recombination render their application. To overcome these drawbacks of Cu_2O, heterojunctions with suitable components have been formed. Among these structures, a new MoS_2-Cu_2O heterostructure was fabricated by Singh et al. Here two types of MoS_2, p-MoS_2 and n-MoS_2, were used to form heterostructures with CuO: Cu_2O-c (cubic morphology) and Cu_2O-co (cuboctahedron morphology). This new system exhibited both CO_2 reduction and water oxidation capacity. Among these structures, the p-MoS_2/Cu_2O-c type system showed higher activity, following a Z-scheme charge transfer to yield CH_3OH, and DFT calculations further confirm it.[197] Recently, MoS_2-rods/TiO_2 nanotubes (NTs) heterojunction was introduced for exploiting photoenhanced electrocatalytic reduction (PEEC) of CO_2 to methanol.

The resulting composite exhibited excellent optical performance but had an unmatched conduction band minimum (CBM) of −0.15 eV with low Faradaic efficiency. Therefore, developed a new PEEC to reduce CO_2 to methanol on MoS_2-rods/TiO_2 NTs. Adding illumination to the electrocatalytic system improved the Faradaic efficiency to 111.58% more than the same electrocatalytic (EC) system. They introduced a unique mechanism for the PEEC reduction of CO_2 to methanol. The reduction of CO_2 to CH_3OH consists of six electronic reactions, as shown in Figure 13a. On one side, when applying −1.3 V potential on the cathode, the anode potential is 1.82 V versus SCE and can oxidize H_2O to O_2 and protons. Then the protons will reach the cathode for CO_2 EC reduction. Moreover, the catalyst has a valence band (VB) suitable for in situ PC oxidation of H_2O to generate protons. So, it provides more protons for EC reduction of CO_2 to methanol with high efficiency (Figure 13b).[198] Table 4 summarizes the recent progress in photocatalytic CO_2 reduction using MoS_2 nanocomposites.

4. CONCLUSIONS AND PERSPECTIVES

This review focused on 2D layered MoS_2-based nanostructures for photocatalytic H_2 evolution and CO_2 reduction to hydrocarbon fuels, which have been discussed in the literature over the past several years.

The layered structure of MoS_2 with more active edge sites mainly contributed to its photocatalytic activity. The first part of this review illustrates the H_2 evolution reactions of binary and ternary composites of MoS_2. Binary composites cover the composites of MoS_2 with metal oxides, carbonaceous materials, metal sulfides, and metal−organic frameworks, and ternary heterosystems comprise the combinations of different binary structures with MoS_2. Many studies have shown that combining MoS_2 as a cocatalyst can overcome the barriers to H_2 evolution in many systems. The recombination of charge carriers in several metal oxides is reduced by forming binary structures with MoS_2, where the tuning of the band gap of metal oxide was achieved.[60] The 2D/2D binary heterostructures formed with MoS_2 and carbonaceous materials provide a high surface area that significantly benefits higher H_2 evolution activity. Especially the H_2 production was increased to a large extent by introducing thinner and fluffier flowerlike MoS_2 structures in the framework of gC_3N_4 nanosheets.[76,77] The significant drawbacks like photocorrosion and fast electron−hole recombination of metal sulfides can be effectively eliminated by forming binary structures with MoS_2. Binary heterostructures formed with multimetal sulfides like $ZnIn_2S_4$, $CuInS_2$, and $MgIn_2S_4$ with MoS_2 are also widely used as a photocatalyst for H_2 production. The flowerlike morphology of MoS_2 provides an excellent platform for catalytic activity.[104,105] The peculiar porous structure of MOFs exhibits many coordination centers for H_2 evolution activity, and the association of MoS_2 further increases its activity. Apart from these binary combinations, MoS_2-based ternary composites have much interest due to their efficient multielectron transport mechanism for H_2 production. In these systems, MoS_2 acts as a channel to accept more photogenerated electrons for combining H^+ to produce H_2 at lower overpotentials.[131,132] Ternary composites of MoS_2 containing noble metals always show a high H_2 evolution rate with excellent stability. Such plasmonic metal hybrid systems with MoS_2 contributed much better photocatalytic activity than others. For example, an Au-deposited MoS_2/ZnO system exhibited the highest H_2 evolution rate with good stability.[148]

Though encouraging progress has been achieved toward photocatalytic H_2 evolution using MoS_2-based nanocomposites, some problems and challenges still exist. One of the crucial difficulties is that MoS_2 alone has negligible photocatalytic activity, and its bulk form is an indirect-band gap semiconductor. The band structure of MoS_2 varies with the number of layers. When it became a monolayer, it gave a high optical absorption coefficient and showed better HER performance. Therefore, more research is needed to explore single-layer MoS_2 as a hydrogen evolution catalyst. The combinations of MoS_2 with other transition metal dichalcogenides (TMDs) such as WS_2, $MoSe_2$, and WSe_2 would give much better activity. For example, the WS_2-MoS_2 binary structure with CdS was an efficient noble-metal-free catalyst with high durability. So, the development of such type of hybrid metal sulfide combinations would be more acceptable.[199]

Furthermore, a few reports are available using MoS_2 with inorganic compounds like Mxenes, giving the highest H_2 evolution rate.[126] Similar results were obtained for the 3D structure of graphene containing MoS_2. In this context, efforts for efficient photocatalysts are also to be developed with different compositions for enhanced H_2 evolution performance.[79] In most cases, H_2 evolution occurs in aqueous solutions using diverse sacrificial reagents like triethanolamine, lactic acid, Na_2S-Na_2SO_3 pair, and methanol as electron donors. The use of such sacrificial reagents in MoS_2-based nanocomposites for H_2 evolution implied a higher cost for future applications on a large scale. So, it is essential to develop MoS_2-based photocatalysts for H_2 production without using additional sacrificial reagents.

Photocatalytic CO_2 reduction to hydrocarbon fuels mainly involves multielectron transfer mechanisms and includes a variety of redox potentials. As a result, several products can be generated during the photocatalytic CO_2 reduction process, and the product selectivity is related to the chemical pathways of the reaction. Thus, the role of MoS_2 in photocatalytic CO_2 reduction must be better understood to improve selectivity for a particular fuel. Layered MoS_2 has been widely employed to improve photocatalytic H_2-production performance. However, research on MoS_2-based photocatalysts for CO_2 reduction is still in the early stages. Efforts in developing layered MoS_2-based photocatalysts capable of simultaneous H_2 evolution and CO_2 conversion are an area of current interest.[185,187] Besides the photochemical conversion of CO_2, MoS_2-based systems for CO_2 reduction using photoelectrochemical splitting are highly

https://doi.org/10.1021/acsomega.3c02084
ACS Omega 2023, 8, 25649−25673

required due to their high Faradaic efficiency. Theoretical studies stimulate the electronic properties of MoS_2-nanocomposites, which will help one to understand the efficiency of the catalyst in photoelectrochemical studies.[197,198] In short, developing 2D layered MoS_2-based nanocomposites is a substantial breakthrough in photocatalytic H_2 evolution and CO_2 reduction.

AUTHOR INFORMATION

Corresponding Author

Suresh Mathew − *School of Chemical Sciences, Mahatma Gandhi University, Kottayam, Kerala 686 560, India; Advanced Molecular Materials Research Centre (AMMRC), Mahatma Gandhi University, Kottayam, Kerala 686 560, India;* orcid.org/0000-0002-7461-3438; Email: sureshmathewmgu@gmail.com

Authors

Bhagyalakshmi Balan − *School of Chemical Sciences, Mahatma Gandhi University, Kottayam, Kerala 686 560, India*

Marilyn Mary Xavier − *School of Chemical Sciences, Mahatma Gandhi University, Kottayam, Kerala 686 560, India;* Present Address: Assistant Professor, Department of Chemistry, Morning Star Home Science College, Angamali South, Kerala 683573, India

Complete contact information is available at: https://pubs.acs.org/10.1021/acsomega.3c02084

Notes

The authors declare no competing financial interest.

ACKNOWLEDGMENTS

We are grateful for the financial support of the University Grants Commission (UGC), India. We also thank Gladiya Mani, Sreerenjini C. R., Sithara Gopinath, and Aswathy V. Kumar for fruitful discussions (Mahatma Gandhi University, Kottayam, Kerala).

REFERENCES

(1) Chen, X.; Shen, S.; Guo, L.; Mao, S. S. Semiconductor Based Photocatalytic Hydrogen Generation. *Chem. Rev.* **2010**, *110*, 6503−6570.

(2) Fan, W.; Zhang, Q.; Wang, Y. Semiconductor-Based Nanocomposites for Photocatalytic H_2 Production and CO_2 Conversion. *Phys. Chem. Chem. Phys.* **2013**, *15*, 2632−2649.

(3) Kamat, P. V.; Bisquert, J. Solar Fuels. Photocatalytic Hydrogen Generation. *J. Phys. Chem. C* **2013**, *117*, 14873−14875.

(4) Xiang, Q.; Cheng, B.; Yu, J. Graphene-Based Photocatalysts for Solar-Fuel Generation. *Angew. Chem.* **2015**, *54*, 11350−11366.

(5) Tahir, M. Photocatalytic Carbon Dioxide Reduction to Fuels in Continuous Flow Monolith Photoreactor using Montmorillonite Dispersed Fe/TiO_2Nanocatalyst. *J. Clean. Prod.* **2018**, *170*, 242−250.

(6) Chen, X.; Jin, F. Photocatalytic Reduction of Carbon Dioxide by Titanium Based Semiconductors to Produce Fuels. *Front. Energy Res.* **2019**, *13*, 207−220.

(7) Kumar, S.; Kumar, A.; Kumar, A.; Krishnan, V. Nanoscale Zinc Oxide Based Heterojunctions as Visible Light Active Photocatalysts for Hydrogen Energy and Environmental Remediation. *Catal. Rev. Sci. Eng.* **2020**, *62*, 346−405.

(8) Yadav, A. A.; Hunge, Y. M.; Kang, S. W. Spongy Ball-Like Copper Oxide Nanostructure Modified by Reduced Graphene Oxide for Enhanced Photocatalytic Hydrogen Production. *Mater. Res. Bull.* **2021**, *133*, 111026.

(9) Zhang, Z.; Bian, L.; Tian, H.; Liu, Y.; Bando, Y.; Yamauchi, Y.; Wang, Z. L. Tailoring the Surface and Interface Structures of Copper-Based Catalysts for Electrochemical Reduction of CO_2 to Ethylene and Ethanol. *Small.* **2022**, *18*, 2107450.

(10) Luo, M.; Yang, J.; Li, X.; Eguchi, M.; Yamauchi, Y.; Wang, Z. L. (2023). Insights into Alloy/Oxide or Hydroxide Interfaces in Ni-Mo-Based Electrocatalysts for Hydrogen Evolution Under Alkaline Conditions. *Chem. Sci.* **2023**, *14*, 3400−3414.

(11) Guo, C.; Tian, K.; Wang, L.; Liang, F.; Wang, F.; Chen, D.; Ning, J.; Zhong, Y.; Hu, Y. Approach of Fermi Level and Electron Tap-Level in Cadmium Sulfide Nanorods via Molybdenum Doping with Enhanced Carrier Separation for Boosted Photocatalytic Hydrogen Production. *J. Colloid Interface Sci.* **2021**, *583*, 661−671.

(12) Lyulyukin, M. N.; Kurenkova, A. Y.; Bukhtiyarov, A. V.; Kozlova, E. A. Carbon Dioxide Reduction Under Visible Light: A Comparison of Cadmium Sulfide and Titania Photocatalysts. *Mendeleev Commun.* **2020**, *30*, 192−194.

(13) Wang, H.; Li, S.; Wan, Q.; Su, X.; Song, T.; Wang, X.; Wang, J. Highly Efficient Solution Exfoliation of Few-layered Molybdenum Disulfide Nanosheets for Photocatalytic Hydrogen Evolution. *J. Colloid Interface Sci.* **2020**, *577*, 38−47.

(14) Sasan, K.; Lin, Q.; Mao, C.; Feng, P. Open Framework Metal Chalcogenides as Efficient Photocatalysts for Reduction of CO_2 into Renewable Hydrocarbon Fuel. *Nanoscale.* **2016**, *8*, 10913−10916.

(15) Liu, S.; Jiang, T.; Fan, M.; Tan, G.; Cui, S.; Shen, X. Nanostructure Rod-like TiO_2-Reduced Graphene Oxide Composite Aerogels for Highly Efficient Visible Light Photocatalytic CO_2 Reduction. *J. Alloys Compd.* **2021**, *861*, 158598.

(16) Jiang, L.; Li, J.; Wang, K.; Zhang, G.; Li, Y.; Wu, X. Low Boiling Point Solvent Mediated Strategy to Synthesize Functionalized Monolayer Carbon Nitride for Superior Photocatalytic Hydrogen Evolution. *Appl. Catal., B* **2020**, *260*, 118181.

(17) Tian, L.; Min, S.; Wang, F.; Zhang, Z. Enhanced Photocatalytic Hydrogen Evolution on TiO_2 Employing Vanadium Carbide as an Efficient and Stable Co-catalyst. *Int. J. Hydrog. Energy.* **2020**, *45*, 1878−1889.

(18) Wu, Z.; Li, C.; Li, Z.; Feng, K.; Cai, M.; Zhang, D.; Wang, S.; Chu, M.; Zhang, C.; Shen, J.; Huang, Z.; Xiao, Y.; Ozin, G. A.; Zhang, X.; He, L. Niobium and Titanium Carbides (MXenes) as Superior Photothermal Supports for CO_2 Photocatalysis. *ACS Nano* **2021**, *15*, 5696−5705.

(19) Wang, Z.-L.; Choi, J.; Xu, M.; Hao, X.; Zhang, H.; Jiang, Z.; Zuo, M.; Kim, J.; Zhou, W.; Meng, X.; Yu, Q.; Sun, Z.; Wei, S.; Ye, J.; Wallace, G. G.; Officer, D. L.; Yamauchi, Y. Optimizing Electron Densities of Ni-N-C Complexes by Hybrid Coordination for Efficient Electrocatalytic CO_2 Reduction. *ChemSusChem.* **2020**, *13*, 929−937.

(20) Duplock, E. J.; Scheffler, M.; Lindan, P. J. Hallmark of Perfect Graphene. *Phys. Rev. Lett.* **2004**, *92*, 225502.

(21) Novoselov, K. S.; Geim, A. K.; Morozov, S. V.; Jiang, D.; Katsnelson, M. I.; Grigorieva, I. V.; Dubonos, S. V.; Firsov, A. A. Two-dimensional Gas of Massless Dirac Fermions in Graphene. *Nature.* **2005**, *438*, 197−200.

(22) Lou, Q.; Lou, G.; Peng, R.; Liu, Z.; Wang, W.; Ji, M.; Chen, C.; Zhang, X.; Liu, C.; Ge, Z. Synergistic Effect of Lewis Base Polymers and Graphene in Enhancing the Efficiency of Perovskite Solar Cells. *ACS Appl. Energy Mater.* **2021**, *4*, 3928−3936.

(23) Reynard, D.; Nagar, B.; Girault, H. Photonic Flash Synthesis of Mo_2C/Graphene Electrocatalyst for the Hydrogen Evolution Reaction. *ACS Catal.* **2021**, *11*, 5865−5872.

(24) Wang, H.; Liu, G.; Chen, C.; Tu, W.; Lu, Y.; Wu, S.; O'Hare, D.; Xu, R. Single-Ni Sites Embedded in Multilayer Nitrogen-Doped Graphene Derived from Amino-Functionalized MOF for Highly Selective CO_2 Electroreduction. *ACS Sustain. Chem. Eng.* **2021**, *9*, 3792−3801.

(25) Liu, L.; Dong, R.; Ye, D.; Lu, Y.; Xia, P.; Deng, L.; Duan, Y.; Cao, K.; Chen, S. Phosphomolybdic Acid-Modified Monolayer Graphene Anode for Efficient Organic and Perovskite Light-Emitting Diodes. *ACS Appl. Mater. Interfaces.* **2021**, *13*, 12268−12277.

https://doi.org/10.1021/acsomega.3c02084
ACS Omega 2023, 8, 25649−25673

(26) Tang, Z.; Liu, C.; Huang, X.; Zeng, S.; Liu, L.; Li, J.; Jiang, Y.-G.; Zhang, D. W.; Zhou, P. A Steep-Slope MoS_2/Graphene Dirac-Source Field-Effect Transistor with a Large Drive Current. *Nano Lett.* **2021**, *21*, 1758−1764.
(27) Wang, Y.; Ho, V. X.; Pradhan, P.; Cooney, M. P.; Vinh, N. Q. Interfacial Photogating Effect for Hybrid Graphene-Based Photodetectors. *ACS Appl. Nano Mater.* **2021**, *4*, 8539−8545.
(28) Xie, J.; Zhang, H.; Li, S.; Wang, R.; Sun, X.; Zhou, M.; Zhou, J.; Lou, X. W. D.; Xie, Y. Defect-Rich MoS_2 Ultra-Thin Nanosheets with Additional Active Edge Sites for Enhanced Electrocatalytic Hydrogen Evolution. *Adv. Mater.* **2013**, *25*, 5807−5813.
(29) Das, S.; Chen, H. Y.; Penumatcha, A. V.; Appenzeller, J. High-Performance Multilayer MoS_2Transisters with Scandium Contacts. *J. Nano Lett.* **2013**, *13*, 100−105.
(30) Benck, J. D.; Hellstern, T. R.; Kibsgaard, J.; Chakthranont, P.; Jaramillo, T. F. Catalyzing the Hydrogen Evolution Reaction (HER) with Molybdenum Sulfide Nanomaterials. *ACS Catalysis.* **2014**, *4*, 3957−3971.
(31) Xing, F.; Wang, C.; Liu, S.; Jin, S.; Jin, H.; Li, J. Interfacial Chemical Bond Engineering in a Direct Z-Scheme g-C_3N_4/MoS_2 Heterojunction. *ACS Appl. Mater. Interfaces.* **2023**, *15*, 11731−11740.
(32) Chen, L.; Arshad, M.; Chuang, Y.; Nguyen, T. B.; Wu, C. H.; Chen, C. W.; Dong, C. D. A Novel Nano-heterojunction MoS_2/α-Fe_2O_3 Photocatalysts with High Photocatalytic and Photoelectrochemical Performance under Visible Light Irradiation. *J. Alloys Compd.* **2023**, *947*, 169577.
(33) Wu, C.; Huang, W.; Liu, H.; Lv, K.; Li, Q. Insight into Synergistic Effect of Ti_3C_2 MXene and MoS_2 on Anti-Photocorrosion and Photocatalytic of CdS for Hydrogen Production. *Appl. Catal. B: Environ.* **2023**, *330*, 122653.
(34) Wang, Y.; Yang, C.; Guo, L.; Yang, Z.; Jin, B.; Du, R.; Fu, F.; Wang, D. Plate-on-plate Structured MoS_2/$Cd_{0.6}Zn_{0.4}S$ Z-Scheme Heterostructure with Enhanced Photocatalytic Hydrogen Production Activity via Hole Sacrificial Agent Synchronously Strengthen Half-Reactions. *J. Colloid Interface Sci.* **2023**, *630*, 341−351.
(35) Yang, X.; Lan, X.; Zhang, Y.; Li, H.; Bai, G. Rational Design of MoS_2@COF Hybrid Composites Promoting CC Coupling for Photocatalytic CO_2 Reduction to Ethane. *Appl. Catal. B: Environ.* **2023**, *325*, 122393.
(36) Nair Gopalakrishnan, V.; Becerra, J.; Mohan, S.; Ahad, J. M.; Béland, F.; Do, T. O. Cobalt-Doped MoS_2-Integrated Hollow Structured Covalent Organic Framework Nanospheres for the Effective Photoreduction of CO_2 under Visible Light. *Energy amp; Fuels* **2023**, *37*, 2329−2339.
(37) Hisatomi, T.; Kubota, J.; Domen, K. Recent Advances in Semiconductors for Photocatalytic and Photoelectrochemical Water Splitting. *Chem. Soc. Rev.* **2014**, *43*, 7520−7535.
(38) Tollefson, J. Hydrogen Vehicles: Fuel of the Future? *Nature News.* **2010**, *464*, 1262−1264.
(39) Yuan, Y. J.; Lu, H. W.; Yu, Z. T.; Zou, Z. G. Noble-Metal-Free Molybdenum Disulfide Cocatalyst for Photocatalytic Hydrogen Production. *ChemSusChem.* **2015**, *8*, 4113−4127.
(40) Corredor, J.; Rivero, M. J.; Rangel, C. M.; Gloaguen, F.; Ortiz, I. Comprehensive Review and Future Perspectives on the Photocatalytic Hydrogen Production. *J. Chem. Technol. Biotechnol.* **2019**, *94*, 3049−3063.
(41) Fujishima, A.; Honda, K. Electrochemical Photolysis of Water at a Semiconductor Electrode. *Nature.* **1972**, *238*, 37−38.
(42) Sharma, R.; Almasi, M.; Nehra, S. P.; Rao, V. S.; Panchal, P.; Paul, D. R.; Jain, I. P.; Sharma, A. Photocatalytic Hydrogen Production using Graphitic Carbon Nitride (GCN): A Precise Review. *Renew. Sust. Energy Rev.* **2022**, *168*, 112776.
(43) Han, B.; Hu, Y. H. MoS_2 as a Co-catalyst for Photocatalytic Hydrogen Production from Water. *Energy Sci. Eng.* **2016**, *4*, 285−304.
(44) Ding, Q.; Song, B.; Xu, P.; Jin, S. Efficient Electrocatalytic and Photoelectrochemical Hydrogen Generation Using MoS_2 and Related Compounds. *Chem.* **2016**, *1*, 699−726.
(45) Xu, J.; Shao, G.; Tang, X.; Lv, F.; Xiang, H.; Jing, C.; Zhou, Z. Frenkel-Defected Monolayer MoS_2 Catalysts for Efficient Hydrogen Evolution. *Nat. Commun.* **2022**, *1*, 1−8.
(46) Eknapakul, T.; King, P. D. C.; Asakawa, M.; Buaphet, P.; He, R.-H.; Mo, S.-K.; Takagi, H.; Shen, K. M.; Baumberger, F.; Sasagawa, T.; Jungthawan, S.; Meevasana, W. Electronic Structure of a Quasi-Freestanding MoS_2 Monolayer. *Nano Lett.* **2014**, *14*, 1312−1316.
(47) Ding, Q.; Song, B.; Xu, P.; Jin, S. Efficient Electrocatalytic and Photoelectrochemical Hydrogen Generation Using MoS_2 and Related Compounds. *Chem.* **2016**, *1*, 699−726.
(48) Xiang, Q.; Yu, J.; Jaroniec, M. Synergetic Effect of MoS_2 and Graphene as Co-catalysts for Enhanced Photocatalytic H_2 Production Activity of TiO_2 Nanoparticles. *J. Am. Chem. Soc.* **2012**, *134*, 6575−6578.
(49) Wang, Y.; Wang, Q.; Zhan, X.; Wang, F.; Safdar, M.; He, J. Visible Light-Driven Type II Heterostructures and their Enhanced Photocatalysis Properties: A Review. *Nanoscale.* **2013**, *5*, 8326−8339.
(50) Kadantsev, E. S.; Hawrylak, P. Electronic Structure of a Single MoS_2 Monolayer. *Solid State Commun.* **2012**, *152*, 909−913.
(51) Wang, F.; Shifa, T. A.; Zhan, X.; Huang, Y.; Liu, K.; Cheng, Z.; Jiang, C.; He, J. Recent Advances in Transition-metal Dichalcogenide Based Nanomaterials for Water Splitting. *Nanoscale.* **2015**, *7*, 19764−19788.
(52) Kubacka, A.; Fernandez-Garcia, M.; Colon, G. Advanced Nanoarchiectures for Solar Photocatalytic Applications. *Chem. Rev.* **2012**, *112*, 1555−1614.
(53) Hinnemann, B.; Moses, P. G.; Bonde, J.; Jørgensen, K. P.; Nielsen, J. H.; Horch, S.; Chorkendorff, I.; Nørskov, J. K. Biomimetic Hydrogen Evolution: MoS_2 Nanoparticles as Catalysts for Hydrogen Evolution. *J. Am. Chem. Soc.* **2005**, *127*, 5308−5309.
(54) Bonde, J.; Moses, P. G.; Jaramillo, T. F.; Nørskov, J. K.; Chorkendorff, I. Hydrogen Evolution on Nano-particulate Transition Metal Sulfides. *Faraday Discuss.* **2009**, *140*, 219−231.
(55) Tsai, C.; Chan, K.; Abild-Pedersen, F.; Nørskov, J. K. Active Edge-Sites in $MoSe_2$ and WSe_2 Catalysts for Hydrogen Evolution Reaction: A Density Functional Study. *Phys. Chem. Chem. Phys.* **2014**, *16*, 13156−13164.
(56) Jaramillo, T. F.; Jørgensen, K. P.; Bonde, J.; Nielsen, J. H.; Horch, S.; Chorkendorff, I. Identification of Active Edge Sites for Electrochemical H_2 Evolution from MoS_2 Nanocatalysts. *Science.* **2007**, *317*, 100−102.
(57) Khalid, N. R.; Israr, Z.; Tahir, M. B.; Iqbal, T. Highly Efficient Bi_2O_3/MoS_2 on Heterojunction Photocatalysts for Hydrogen Evolution from Water Splitting. *Int. J. Hydrog. Energy.* **2020**, *45*, 8479−8489.
(58) Pramoda, K.; Servottam, S.; Kaur, M.; Rao, C. N. R. Layered Nanocomposites of Polymer-Functionalized Reduced Graphene Oxide and Borocarbonitride with MoS_2 and $MoSe_2$ and Their Hydrogen Evolution Reaction Activity. *ACS Applied Nano Materials.* **2020**, *3*, 1792−1799.
(59) Wang, W.; Zhu, S.; Cao, Y.; Tao, Y.; Li, X.; Pan, D.; Phillips, D. L.; Zhang, D.; Chen, M.; Li, G.; Li, H. Edge Enriched Ultrathin MoS_2 Embedded Yolk-Shell TiO_2 with Boosted Charge Transfer for Superior Photocatalytic H_2 Evolution. *Adv. Funct. Mater.* **2019**, *29*, 1901958.
(60) Zhou, X.; Lickleder, M.; Schmuki, P. Thin MoS_2 on TiO_2 Nanotube Layers: An Efficient Co-catalyst/Harvesting System for Photocatalytic H_2 Evolution. *Electrochem. Commun.* **2016**, *73*, 33−37.
(61) Agrawal, A. V.; Kumar, R.; Venkatesan, S.; Zakhidov, A.; Yang, G.; Bao, J.; Kumar, M.; Kumar, M. Photoactivated Mixed In-Plane and Edge-Enriched p-Type MoS_2 Flake-Based NO_2 Sensor Working at Room Temperature. *ACS Sens.* **2018**, *3*, 998−1004.
(62) Zhu, Y.; Ling, Q.; Liu, Y.; Wang, H.; Zhu, Y. Photocatalytic H_2 Evolution on MoS_2-TiO_2 Catalysts Synthesized via Mechanochemistry. *Phys. Chem. Chem. Phys.* **2015**, *17*, 933−940.
(63) Kumar, S.; Kumar, A.; Navakoteswara Rao, V.; Kumar, A.; Shankar, M. V.; Krishnan, V. Defect-Rich MoS_2 Ultrathin Nanosheets-Coated Nitrogen-Doped ZnO Nanorod Heterostructures: An

https://doi.org/10.1021/acsomega.3c02084
ACS Omega 2023, 8, 25649−25673

Insight into in-situ-Generated ZnS for Enhanced Photocatalytic Hydrogen Evolution. *ACS Appl. Energy Mater.* **2019**, *2*, 5622−5634.
(64) Yuan, Y.-J.; Wang, F.; Hu, B.; Lu, H. W.; Yu, Z. T.; Zou, Z. G. Significant Enhancement in Photocatalytic Hydrogen Evolution from Water Using MoS_2-Nanosheet-Coated ZnO Heterostructure Photocatalyst. *Dalton Trans.* **2015**, *44*, 10997−11003.
(65) Yuan, Y.-J.; Tu, J.-R.; Ye, Z.-J.; Lu, H.-W.; Ji, Z.-G.; Hu, B.; Li, Y.-H.; Cao, D.-P.; Yu, Z.-T.; Zou, Z.-G. Visible-Light-Driven Hydrogen Production from in a Noble-Metal-Free System Catalyzed by Zinc Porphyrin Sensitized MoS_2/ZnO. *Dyes Pigm.* **2015**, *123*, 285−292.
(66) Shu, X.; Zhao, C.; Zhang, X.; Liu, X.; Xing, Z.; Fang, D.; Wang, J.; Song, Y. Highly Efficient Near-Infrared Light Photocatalytic Hydrogen Evolution Over MoS_2 Supported Ta_2O_5 Combined with an Up-Conversion Luminescence Agent β-Tm^{3+}, Yb^{3+}: $NaYF_4$/MoS_2-Ta_2O_5 Nanocomposite. *New J. Chem.* **2018**, *42*, 6134−6143.
(67) Goud, B. S.; Koyyada, G.; Jung, J. H.; Reddy, G. R.; Shim, J.; Nam, N. D.; Vattikuti, S. P. Surface Oxygen Vacancy Facilitated Z-Scheme MoS_2/Bi_2O_3 Heterojunction for Enhanced Visible-Light Driven Photocatalysis-Pollutant Degradation and Hydrogen Production. *Int. J. Hydrog. Energy.* **2020**, *45*, 18961−18975.
(68) Ye, L.; Xu, H.; Zhang, D.; Chen, S. Synthesis of Bilayer MoS_2 Nanosheets by a Facile Hydrothermal Method, and their Methyl Orange Adsorption Capacity. *Mater. Res. Bull.* **2014**, *55*, 221−228.
(69) Opoku, F.; Govender, K. K.; van Sittert, C. G. C. E.; Govender, P. P. Role of MoS_2 and WS_2 Monolayers on Photocatalytic Hydrogen Production and the Pollutant Degradation of $BiVO_4$: A First-principles Study. *New J. Chem.* **2017**, *41*, 11701−11713.
(70) Swain, G.; Sultana, S.; Naik, B.; Parida, K. Coupling of Crumpled-Type Novel MoS_2 with CeO_2 Nanoparticles: A Noble-Metal-Free p-n Heterojunction Composite for Visible Light Photocatalytic H_2 Production. *ACS Omega.* **2017**, *2*, 3745−3753.
(71) Deng, D.; Novoselov, K. S.; Fu, Q.; Zheng, N.; Tian, Z.; Bao, X. Catalysis with Two-Dimensional Materials and their Heterostructures. *Nat. Nanotechnol.* **2016**, *11*, 218−230.
(72) Yin, M.; Sun, J.; Li, Y.; Ye, Y.; Liang, K.; Fan, Y.; Li, Z. Efficient photocatalytic Hydrogen Evolution Over MoS_2/Activated Carbon Composite Sensitized by Erythrosin B Under LED Light Irradiation. *Catal. Commun.* **2020**, *142*, 106029.
(73) Koutsouroubi, E. D.; Vamvasakis, I.; Papadas, I. T.; Drivas, C.; Choulis, S. A.; Kennou, S.; Armatas, G. S. Interface Engineering of MoS_2-Modified Graphitic Carbon Nitride Nano-Photocatalysts for an Efficient Hydrogen Evolution Reaction. *ChemPlusChem.* **2020**, *85*, 1379−1388.
(74) Li, N.; Zhou, J.; Sheng, Z.; Xiao, W. Molten Salt-Mediated formation of g-C_3N_4-MoS_2 for Visible-Light-Driven Photocatalytic Hydrogen Evolution. *Appl. Surf. Sci.* **2018**, *430*, 218−224.
(75) Zheng, D.; Zhang, G.; Hou, Y.; Wang, X. Layering MoS_2 on Soft Hollow g-C_3N_4 Nanostructures for Photocatalytic Hydrogen Evolution. *APPL CATAL A-GEN.* **2016**, *521*, 2−8.
(76) Ge, L.; Han, C.; Xiao, X.; Guo, L. Synthesis and Characterization of Composite Visible Light Active Photocatalysts MoS_2-g-C_3N_4 with Enhanced Hydrogen Evolution Activity. *Int. J. Hydrog. Energy.* **2013**, *38*, 6960−6969.
(77) Liu, Y.; Xu, X.; Zhang, J.; Zhang, H.; Tian, W.; Li, X.; Tade, M. O.; Sun, H.; Wang, S. Flower-Like MoS_2 on Graphitic Carbon Nitride for Enhanced Photocatalytic and Electrochemical Hydrogen Evolutions. *Appl. Catal., B* **2018**, *239*, 334−344.
(78) Yuan, Y.-J.; Shen, Z.; Wu, S.; Su, Y.; Pei, L.; Ji, Z.; Ding, M.; Bai, W.; Chen, Y.; Yu, Z.-T.; Zou, Z. Liquid Exfoliation of g-C_3N_4 Nanosheets to Construct 2D-2D MoS_2/g-C_3N_4 Photocatalysts for Enhanced Photocatalytic Hydrogen Production Activity. *Appl. Catal., B* **2019**, *246*, 120−128.
(79) Li, X.; Guo, S.; Li, W.; Ren, X.; Su, J.; Song, Q.; Sobrido, A. J.; Wei, B. Edge-Rich MoS_2 Grown on Edge-Oriented Three-Dimensional Graphene Glass for High-Performance Hydrogen Evolution. *Nano Energy.* **2019**, *57*, 388−397.
(80) Masimukku, S.; Tsai, D. L.; Lin, Y. T.; Chang, I. L.; Wu, J. J. Low-Frequency Vibration Induced Piezoelectric Boost to Photocatalytic Hydrogen Evolution through 2D-2D-Stacked MoS_2-Carbon Nitride. *Appl. Surf. Sci.* **2023**, *614*, 156147.
(81) Li, Y.; Chen, G.; Zhou, C.; Sun, J. A Simple-Template-Free Synthesis of Nanoporous ZnS-In_2S_3-Ag_2S Solid Solutions for Highly Efficient Photocatalytic H_2 Evolution Under Visible Light. *Chem-Comm.* **2009**, *15*, 2020−2022.
(82) Kadam, S. R.; Panmand, R. P.; Sonawane, R. S.; Gosavi, S. W.; Kale, B. B. A Stable Bi_2S_3-Quantum Dot-Glass Nanosystem: Size Tunable Photocatalytic Hydrogen Production Under Solar Light. *RSC Adv.* **2015**, *5*, 58485−58490.
(83) Wang, Q.; An, N.; Bai, Y.; Hang, H.; Li, J.; Lu, X.; Liu, Y.; Wang, F.; Li, Z.; Lei, Z. High Photocatalytic Hydrogen Production from Methanol Aqueous Solution Using the Photocatalysts CuS/TiO_2. *Int. J. Hydrog. Energy.* **2013**, *38*, 10739−10745.
(84) Li, L.-L.; Yin, X.-L.; Pang, D.-H.; Du, X.-X.; Xue, H.; Zhou, H.-W.; Yao, Q.-X.; Wang, H.-W.; Qian, J.-C.; Yang, J.; Li, D.-C.; Dou, J.-M. One-Pot Synthesis of MoS_2/CdS Nanosphere Heterostructures for Efficient H_2 Evolution Under Visible Light Irradiation. *Int. J. Hydrog. Energy.* **2019**, *44*, 31930−31939.
(85) Lv, Y.; Chen, P.; Foo, J. J.; Zhang, J.; Qian, W.; Chen, C.; Ong, W. J. Dimensionality-Dependent MoS_2 toward Efficient Photocatalytic Hydrogen Evolution: From Synthesis to Modifications in Doping, Surface, and Heterojunction Engineering. *Mater. Today Nano.* **2022**, *18*, 100191.
(86) Xu, X.; Luo, F.; Zhou, G.; Hu, J.; Zeng, H.; Zhou, Y. Self-Assembly Optimization of Cadmium/Molybdenum Sulfide by Cation Coordination Competition Toward Extraordinarily Efficient Photocatalytic Hydrogen Evolution. *J. Mater. Chem. A* **2018**, *6*, 18396−18402.
(87) Ma, S.; Xie, J.; Wen, J.; He, K.; Li, X.; Liu, W.; Zhang, X. Constructing 2D Layered Hybrid CdS Nanosheets/MoS_2 Heterojunctions for Enhanced Visible-Light Photocatalytic H_2 Generation. *Appl. Surf. Sci.* **2017**, *391*, 580−591.
(88) Li, C.; Wang, H.; Ming, J.; Liu, M.; Fang, P. Hydrogen Generation by Photocatalytic Reforming of Glucose with Heterostructured CdS/MoS_2 Composites Under Visible Light Irradiation. *Int. J. Hydrog. Energy.* **2017**, *42*, 16968−16978.
(89) Kumar, D. P.; Seo, S.; Rangappa, A. P.; Kim, S.; Joshi Reddy, K. A.; Gopannagari, M.; Bhavani, P.; Reddy, D. A.; Kim, T. K. Ultrathin layered Zn-doped MoS_2 nanosheets deposited onto CdS nanorods for spectacular photocatalytic hydrogen evolution. *J. Alloys Compd.* **2022**, *905*, 164193.
(90) Guo, S.; Yang, L.; Zhang, Y.; Huang, Z.; Ren, X.; Sha, W. E. I.; Li, X. Enhanced Hydrogen Evolution via Interlaced Ni_3S_2/MoS_2 Heterojunction Photocatalysts with Efficient Interfacial Contact and Broadband Absorption. *J. Alloys Compd.* **2018**, *749*, 473−480.
(91) Zhao, H.; Fu, H.; Yang, X.; Xiong, S.; Han, D.; An, X. MoS_2/CdS Rod-like Nanocomposites as High-Performance Visible Light Photocatalyst for Water Splitting Photocatalytic Hydrogen Production. *Int. J. Hydrog. Energy.* **2022**, *47*, 8247−8260.
(92) Zhang, K.; Mou, Z.; Cao, S.; Meng, T.; Li, J.; Ling, G.; Zhang, X.; Zhou, Z.; Meng, W. MoS_2 Grown in-situ on CdS Nanosheets for Boosted Photocatalytic Hydrogen Evolution under Visible Light. *Int. J. Hydrog. Energy.* **2022**, *47*, 2967−2975.
(93) Huang, L.; Han, B.; Huang, X.; Liang, S.; Deng, Z.; Chen, W.; Peng, M.; Deng, H. Ultrathin 2D/2D $ZnIn_2S_4$/MoS_2 Hybrids for Boosted Photocatalytic Hydrogen Evolution Under Visible Light. *J. Alloys Compd.* **2019**, *798*, 553−559.
(94) Li, W.; Lin, Z.; Yang, G. A 2D Self-Assembled MoS_2/$ZnIn_2S_4$ Heterostructure for Efficient Photocatalytic Hydrogen Evolution. *Nanoscale.* **2017**, *9*, 18290−18298.
(95) Wang, Y.; Yang, C.; Guo, L.; Yang, Z.; Jin, B.; Du, R.; Fu, F.; Wang, D. Plate-on-Plate Structured MoS_2/$Cd_{0.6}Zn_{0.4}S$ Z-Scheme Heterostructure with Enhanced Photocatalytic Hydrogen Production Activity via Hole Sacrificial Agent Synchronously Strengthen Half-reactions. *J. Colloid Interface Sci.* **2023**, *630*, 341−351.
(96) Fang, H.; Cai, J.; Li, H.; Wang, J.; Li, Y.; Zhou, W.; Mao, K.; Xu, Q. Fabrication of Ultrathin Two-Dimensional/Two-Dimensional MoS_2/$ZnIn_2S_4$ Hybrid Nanosheets for Highly Efficient Visible-Light-

https://doi.org/10.1021/acsomega.3c02084
ACS Omega 2023, 8, 25649−25673

Driven Photocatalytic Hydrogen Evolution. *ACS Appl. Energy Mater.* **2022**, *5*, 8232−8240.
(97) Chand, M.; Rawat, A. S.; Khanuja, M.; Rawat, S. Hydrogen production activity of MoS_2-$ZnIn_2S_4$ Nanocomposite under Visible Light Irradiation. *Mater. Today: Proc.* **2022**, *66*, 1951−1954.
(98) Zhang, Z.; Huang, L.; Zhang, J.; Wang, F.; Xie, Y.; Shang, X.; Gu, Y.; Zhao, H.; Wang, X. In Situ Constructing Interfacial Contact MoS_2/$ZnIn_2S_4$ Heterostructure for Enhancing Solar Photocatalytic Hydrogen Evolution. *Appl. Catal., B* **2018**, *233*, 112−119.
(99) Huang, T.; Chen, W.; Liu, T. Y.; Hao, Q. L.; Liu, X. H. $ZnIn_2S_4$ Hybrid with MoS_2: A Non-noble Metal Photocatalyst with Efficient Photocatalytic Activity for Hydrogen Evolution. *Powder Technol.* **2017**, *315*, 157−162.
(100) Tian, G.; Chen, Y.; Ren, Z.; Tian, C.; Pan, K.; Zhou, W.; Fu, H. Enhanced Photocatalytic Hydrogen Evolution over Hierarchical Composites of $ZnIn_2S_4$ Nanosheets Grown on MoS_2 Slices. *Chem.—Asian J.* **2014**, *9*, 1291−1297.
(101) Wei, L.; Chen, Y.; Lin, Y.; Wu, H.; Yuan, R.; Li, Z. MoS_2 as Non-Noble-Metal Co-catalyst for Photocatalytic Hydrogen Evolution over Hexagonal $ZnIn_2S_4$ Under Visible Light Irradiations. *Appl. Catal., B* **2014**, *144*, 521−527.
(102) Swain, G.; Parida, K. Design of a Novel p-MoS_2@n-$ZnIn_2S_4$ Heterojunction Based Semiconducting Photocatalyst Towards Photocatalytic HER. *Mater. Today: Proc.* **2021**, *35*, 268−274.
(103) Pudkon, W.; Bahruji, H.; Miedziak, P. J.; Davies, T. E.; Morgan, D. J.; Pattisson, S.; Kaowphong, S.; Hutchings, G. J. Enhanced Visible-Light-Driven Photocatalytic H_2 Production and Cr (VI) Reduction of a ZnI_2S_4/MoS_2 Heterojunction Synthesized by the Bio-molecule Assisted Microwave Heating Method. *Catal. Sci. Technol.* **2020**, *10*, 2838−2854.
(104) Swain, G.; Sultana, S.; Parida, K. Constructing a Novel Surfactant Free MoS_2 Nanosheet Modified $MgIn_2S_4$ Marigold Microflower: An Efficient Visible-Light-Driven 2D-2D p-n Heterojunction Photocatalyst Toward HER and pH Regulated NRR. *ACS Sustain. Chem. Eng.* **2020**, *8*, 4848−4862.
(105) Swain, G.; Sultana, S.; Moma, J.; Parida, K. Fabrication of Hierarchical Two-Dimensional MoS_2 Nanoflowers Decorated upon Cubic $CaIn_2S_4$ Microflowers: Facile Approach to Construct Novel Metal-Free p-n Heterojunction Semiconductors with Superior Charge Separation Efficiency. *Inorg. Chem.* **2018**, *57*, 10059−10071.
(106) Fan, K.; Jin, Z.; Wang, G.; Yang, H.; Liu, D.; Hu, H.; Lu, G.; Bi, Y. Distinctive Organized Molecular Assemble of MoS_2, MOF, and Co_3O_4, for Efficient Dye-Sensitized Photocatalytic H_2 Evolution. *Catal. Sci. Technol.* **2018**, *8*, 2352−2363.
(107) Jin, Z.; Wang, Z.; Yuan, H.; Han, F. Inseting MOF into flaky CdS Photocatalyst Forming Special Structure and Active Sites for Efficient Hydrogen Production. *Int. J. Hydrog. Energy.* **2019**, *44*, 19640−19649.
(108) Lin, L.; Huang, S.; Zhu, Y.; Du, B.; Zhang, Z.; Chen, C.; Wang, X.; Zhang, N. Construction of CdS/MoS_2 Heterojunction from Core-Shell MoS_2@Cd MOF for Efficient Photocatalytic Hydrogen Evolution. *Dalton Trans.* **2019**, *48*, 2715−2721.
(109) Qiu, J.; Zheng, W.; Yuan, R.; Yue, C.; Li, D.; Liu, F.; Zhu, J. A Novel 3D Nanofibrous Aerogel-Based MoS_2@Co_3S_4 Heterojunction Photocatalyst for Water Remediation and Hydrogen Evolution Under Stimulated Solar Irradiation. *Appl. Catal., B* **2020**, *264*, 118514.
(110) Ma, B.; Chen, T.-T.; Li, Q.-Y.; Qin, H.-N.; Dong, X.-Y.; Zang, S.-Q. Bimetal-Organic-Framework-Derived Nanohybrids $Cu_{0.9}Co_{2.1}S_4$@MoS_2 for High-Performance Visible-Light-Catalytic Hydrogen Evolution Reaction. *ACS Appl. Energy Mater.* **2019**, *2*, 1134−1148.
(111) Qiao, Z.; Wang, W.; Liu, N.; Huang, H.-T.; Karuppasamy, L.; Yang, H.-J.; Liu, C.-H.; Wu, J. J. Synthesis of MOF/MoS_2 Composite Photocatalysts with Enhanced Photocatalytic Performance for Hydrogen Evolution from Water Splitting. *Int. J. Hydrog. Energy.* **2022**, *47*, 40755−40767.
(112) Tahir, M. B. Construction of MoS_2/CND-WO_3 Ternary Composite for Photocatalytic Hydrogen Evolution. *J. Inorg. Organomet. Polym. Mater.* **2018**, *28*, 2160−2168.
(113) Kumar, D. P.; Hong, S.; Reddy, D. A.; Kim, T. K. Ultrathin MoS_2 Layers Anchored Exfoliated Reduced Graphene Oxide Nanosheet Hybrid as a Highly Efficient Co-catalyst for CdS Nanorods Towards Enhanced Photocatalytic Hydrogen Production. *Appl. Catal., B* **2017**, *212*, 7−14.
(114) Zhu, C.; Wang, Y.; Jiang, Z.; Xu, F.; Xian, Q.; Sun, C.; Tong, Q.; Zou, W.; Duan, X.; Wang, S. CeO_2 Nanocrystal Modified Layered MoS_2/g-C_3N_4 as 0D/2D Ternary Composite for Visible Light Photocatalytic Hydrogen Evolution: Interfacial Consecutive Multy-step Electron Transfer and Enhanced H_2O Reactant Adsorption. *Appl. Catal., B* **2019**, *259*, 118072.
(115) Xu, X.; Si, Z.; Liu, L.; Wang, Z.; Chen, Z.; Ran, R.; He, Y.; Weng, D. Co-MoS_2/rGO/C_3N_4 Ternary Heterojunctions Catalysts with High Photocatalytic Activity and Stability for Hydrogen Evolution Under Visible Light Irradiation. *Appl. Surf. Sci.* **2018**, *435*, 1296−1306.
(116) Kumar, S.; Reddy, N. L.; Kushwaha, H. S.; Kumar, A.; Shankar, M. V.; Bhattacharyya, K.; Halder, A.; Krishnan, V. Efficient Electron Transfer Across a ZnO-MoS_2-Reduced Graphene Oxide Heterojunction for Enhanced-Sunlight Driven Photocatalytic Hydrogen Evolution. *ChemSusChem.* **2017**, *10*, 3588−3603.
(117) Reddy, D. A.; Park, H.; Ma, R.; Kumar, D. P.; Lim, M.; Kim, T. K. Heterostructured WS_2-MoS_2 Ultrathin nanosheets Integrated on CdS Nanorods to Promote Charge Separation and Migration and Improve Solar-Driven Photocatalytic Hydrogen Evolution. *ChemSusChem.* **2017**, *10*, 1563−1570.
(118) Choi, J.; Amaranatha Reddy, D.; Han, N. S.; Jeong, S.; Hong, S.; Praveen Kumar, D.; Song, J. K.; Kim, T. K. Modulation of Charge Carrier Pathways in CdS Nanospheres by Integrating MoS_2 and NiP for Improved Migration and Separation Toward Enhanced Photocatalytic Hydrogen Evolution. *Catal. Sci. Technol.* **2017**, *7*, 641−649.
(119) Yu, X.; Du, R.; Li, B.; Zhang, Y.; Liu, H.; Qu, J.; An, X. Biomolecule-Assisted Self-Assembly of CdS/MoS_2/Graphene Hollow Spheres as High-Efficiency Photocatalysts for Hydrogen Evolution without Noble Metals. *Applied Catalysis B: Environmental.* **2016**, *182*, 504−512.
(120) Sasikala, R.; Gaikwad, A. P.; Jayakumar, O. D.; Girija, K. G.; Rao, R.; Tyagi, A. K.; Bharadwaj, S. R. Nanohybrid MoS_2-PANI-CdS Photocatalyst for Hydrogen Evolution from Water. *Colloids Surf, A PhysicochemEng. Asp.* **2015**, *481*, 485−492.
(121) Sun, J.; Maimaiti, H.; Zhai, P.; Zhang, H.; Feng, L.; Bao, J.; Zhao, X. Preparation of a Coal-Based MoS_2/SiO_2/GO Composite Catalyst and Its Performance in the Photocatalytic Degradation of Wastewater and Hydrogen Production. *Langmuir.* **2022**, *38*, 3305−3315.
(122) Dong, J.; Fang, W.; Yuan, H.; Xia, W.; Zeng, X.; Shangguan, W. Few-Layered MoS_2/ZnCdS/ZnS Heterostructures with an Enhanced Photocatalytic Hydrogen Evolution. *ACS Applied Energy Materials.* **2022**, *5*, 4893−4902.
(123) Wang, J.; Zhu, H.; Tang, S.; Li, M.; Zhang, Y.; Xing, W.; Xue, Q.; Yu, L. Sandwich Structure MoO_2/MoS_2/TiO_2 Photocatalyst for Superb Hydrogen Evolution. *J. Alloys Compd.* **2020**, *842*, 155869.
(124) Feng, H. Q.; Xi, Y.; Xie, H. Q.; Li, Y. K.; Huang, Q. Z. An Efficient Ternary $Mn_{0.2}Cd_{0.8}S$/MoS_2/Co_3O_4 Heterojunction for Visible-Light-Driven Photocatalytic Hydrogen Evolution. *Int. J. Hydrog. Energy.* **2020**, *45*, 10764−10774.
(125) Liu, Y.; Xu, C.; Xie, Y.; Yang, L.; Ling, Y.; Chen, L. Au-Cu Nanoalloy/TiO_2/MoS_2 Ternary Hybrid with Enhanced Photocatalytic Hydrogen Production. *J. Alloys Compd.* **2020**, *820*, 153440.
(126) Chen, R.; Wang, P.; Chen, J.; Wang, C.; Ao, Y. Synergistic Effect of MoS_2 and MXene on the Enhanced H_2 Evolution Performance of CdS Under Visible Light Irradiation. *Appl. Surf. Sci.* **2019**, *473*, 11−19.
(127) Wang, B.; Deng, Z.; Fu, X.; Li, Z. MoS_2/CQDs Obtained by Photoreduction for Assembly of a Ternary MoS_2/CQDs/$ZnIn_2S_4$ Nanocomposite for Efficient Photocatalytic Hydrogen Evolution Under Visible Light. *J. Mater. Chem. A* **2018**, *6*, 19735−19742.
(128) Guan, Z.; Wang, P.; Li, Q.; Li, G.; Yang, J. Constructing a $ZnIn_2S_4$ Nanoparticle/MoS_2-RGO Nanosheet 0D/2D Heterojunction

https://doi.org/10.1021/acsomega.3c02084
ACS Omega 2023, 8, 25649−25673

for Significantly Enhanced Visible Light Photocatalytic H_2 Production. *Dalton Trans.* **2018**, *47*, 6800−6807.
(129) Du, J.; Wang, H.; Yang, M.; Zhang, F.; Wu, H.; Cheng, X.; Yuan, S.; Zhang, B.; Li, K.; Wang, Y.; Lee, H. Highly Efficient Hydrogen Evolution Catalysis Based on $MoS_2/CdS/TiO_2$ Porous Composites. *Int. J. Hydrog. Energy.* **2018**, *43*, 9307−9315.
(130) Yuan, Y.-J.; Fang, G.; Chen, D.; Huang, Y.; Yang, L.-X.; Cao, D.-P.; Wang, J.; Yu, Z.-T.; Zou, Z.-G. High Light Harvesting Efficiency $CuInS_2$ quantum dots/TiO_2/MoS_2 Photocatalysts for Enhanced Visible Light Photocatalytic Hydrogen Production. *Dalton Trans.* **2018**, *47*, 5652−5659.
(131) Zhao, H.; Sun, S.; Wu, Y.; Jiang, P.; Dong, Y.; Xu, Z. J. Ternary Graphitic Carbon Nitride/Red Phosphorous/Molybdenum Disulfide Heterostructure: An Efficient and Low-Cost Photocatalyst for Visible-Light -Driven H_2 Evolution from Water. *Carbon.* **2017**, *119*, 56−61.
(132) Qin, N.; Xiong, J.; Liang, R.; Liu, Y.; Zhang, S.; Li, Y.; Li, Z.; Wu, L. Highly Efficient Photocatalytic H_2 Evolution over MoS_2/CdS-TiO_2 Nanofibers Prepared by an Electrospinning Mediated Photoreduction Method. *Appl. Catal., B* **2017**, *202*, 374−380.
(133) Jo, W.-K.; Sagaya Selvam, N. C. Fabrication of Photostable Ternary CdS/MoS_2/MWCNTs Hybrid Photocatalysts with Enhanced H_2 Generation Activity. *Appl. Catal. A Gen.* **2016**, *525*, 9−22.
(134) Jiang, W.; Liu, Y.; Zong, R.; Li, Z.; Yao, W.; Zhu, Y. Photocatalytic Hydrogen Generation on Bifunctional Ternary Heterostructured In_2S_3/MoS_2/CdS Composites with High Activity and Stability Under Visible Light Irradiation. *J. Mater. Chem. A* **2015**, *3*, 18406−18412.
(135) Du, R.; Zhang, Y.; Li, B.; Yu, X.; Liu, H.; An, X.; Qu, J. Biomolecule-Assisted Synthesis of Defect-Mediated $Cd_{1-x}Zn_xS/MoS_2$/Graphene Hollow Spheres for Highly Efficient Hydrogen Evolution. *Phys. Chem. Chem. Phys.* **2016**, *18*, 16208−16215.
(136) Yan, W.; Xu, Y.; Hao, S.; He, Z.; Wang, L.; Wei, Q.; Xu, J.; Tang, H. Promoting Charge Separation in Hollow-Structured C/MoS_2@$ZnIn_2S_4$/Co_3O_4 Photocatalysts via Double Heterojunctions for Enhanced Photocatalytic Hydrogen Evolution. *Inorg. Chem.* **2022**, *61*, 4725−4734.
(137) Xu, Y.; Yan, A.; Jiang, L.; Huang, F.; Hu, D.; Duan, G.; Zheng, F. MoS_2/HCSs/$ZnIn_2S_4$ Nanocomposites with Enhanced Charge Transport and Photocatalytic Hydrogen Evolution Performance. *J. Alloys Compd.* **2022**, *895*, 162504.
(138) Ran, Q.; Yu, Z.; Jiang, R.; Qian, L.; Hou, Y.; Yang, F.; Li, F.; Li, M.; Sun, Q.; Zhang, H. Path Electron Transfer Created in S-Doped NH_2-UiO-66 Bridged $ZnIn_2S_4/MoS_2$ Nanosheet Heterostructure for Boosting Photocatalytic Hydrogen Evolution. *Catal. Sci. Technol.* **2020**, *10*, 2531−2539.
(139) Lin, H.; Sun, B.; Wang, H.; Ruan, Q.; Geng, Y.; Li, Y.; Wu, J.; Wang, W.; Liu, J.; Wang, X. Unique 1D $Cd_{1-x}Zn_xS$@O-MoS_2/NiOx Nanohybrids: Highly Efficient Visible-Light-Driven Photocatalytic Hydrogen Evolution via Integrated Structural Regulation. *Small.* **2019**, *15*, 1804115.
(140) Liu, X.; Wang, B.; Heng, Q.; Chen, W.; Li, X.; Mao, L.; Shangguan, W. Promoted Charge Separation on 3D Interconnected Ti_3C_2/MoS_2/CdS Composite for Enhanced Photocatalytic H2 Production. *Int. J. Hydrog. Energy.* **2022**, *47*, 8284−8293.
(141) Huang, X.; El-Sayed, M. A. Gold Nanoparticles: Optical Properties and Implementations in Cancer Diagnosis and Photothermal Therapy. *J. Adv. Res.* **2010**, *1*, 13−28.
(142) Pany, S.; Naik, B.; Martha, S.; Parida, K. Plasmon Induced Nano Au Particle Decorated over S, N-Modified TiO_2 Exceptional Photocatalytic Hydrogen Evolution Under Visible Light. *ACS Appl. Mater. Interfaces.* **2014**, *6*, 839−846.
(143) Zhang, J.; Liu, M.; Wang, Y.; Shi, F. Au/MoS_2/Ti_3C_2 Composite Catalyst for Efficient Photocatalytic Hydrogen Evolution. *CrystEngComm.* **2020**, *22*, 3683−3691.
(144) Li, S.; Pu, T.; Wang, J.; Fang, X.; Liu, Y.; Kang, S.; Cui, L. Efficient Visible-Light-Driven Hydrogen Evolution over Ternary MoS_2/Pt-TiO_2 Photocatalyst with Low Overpotential. *Int. J. Hydrog. Energy.* **2018**, *43*, 16534−16542.
(145) Wi, D. H.; Park, S. Y.; Lee, S.; Sung, J.; Hong, J. W.; Han, S. W. Metal-Semiconductor Ternary Hybrids for Efficient Visible-Light Photocatalytic Hydrogen Evolution. *J. Mater. Chem. A* **2018**, *6*, 13225−13235.
(146) Huang, T.; Hua, Y.; Yao, J.; Luo, Y.; Liu, X. The Synergetic Effect of Graphene and MoS_2 on AgInZnS for Visible-Light-Driven Photocatalytic H_2 Evolution. *Mater. Chem. Phys.* **2018**, *212*, 506−512.
(147) Chava, R. K.; Do, J. Y.; Kang, M. Smart Hybridization of Au Coupled CdS Nanorods with Few Layered MoS_2 Nanosheets for High-Performance Photocatalytic Hydrogen Evolution Reaction. *ACS Sustain. Chem. Eng.* **2018**, *6*, 6445−6457.
(148) Guo, S.; Li, X.; Zhu, J.; Tong, T.; Wei, B. Au NPs@MoS_2 Sub-Micrometer Sphere-ZnO Nanorod Hybrid Structures for Efficient Photocatalytic Hydrogen Evolution with Excellent Stability. *Small.* **2016**, *12*, 5692−5701.
(149) Cowan, A. J.; Durrant, J. R. Long-Lived Charge Separated States in Nanostructured Semiconductor Photoelectrodes of the Production of Solar Fuels. *Chem. Soc. Rev.* **2013**, *42*, 2281−2293.
(150) Izumi, Y. Recent Advances in the Photocatalytic Conversion of Carbon Dioxide to Fuels with Water and/or Hydrogen Using Solar Energy and Beyond. *Coord. Chem. Rev.* **2013**, *257*, 171−186.
(151) Yu, J.; Low, J.; Xiao, W.; Zhou, P.; Jaroniec, M. Enhanced Photocatalytic CO_2-Reduction Activity of Anatase TiO_2 by Co-exposed {001} and {101} Facets. *J. Am. Chem. Soc.* **2014**, *136*, 8839−8842.
(152) Hoffmann, M. R.; Moss, J. A.; Baum, M. M. Artificial Photosynthesis: Semiconductor Photocatalytic Fixation of CO_2 to Afford Higher Organic Compounds. *Dalton Trans.* **2011**, *40*, 5151−5158.
(153) Sun, H.; Wang, S. Research Advances in the Synthesis of Nanocarbon-Based Photocatalysts and their Applications for Photocatalytic Conversion of Carbon Dioxide to Hydrocarbon Fuels. *Energy Fuels.* **2014**, *28*, 22−36.
(154) Li, X.; Yu, J.; Jaroniec, M.; Chen, X. Cocatalysts for Selective Photoreduction of CO_2 into Solar Fuels. *Chem. Rev.* **2019**, *119*, 3962−4179.
(155) Xiong, Z.; Lei, Z.; Li, Y.; Dong, L.; Zhao, Y.; Zhang, J. A Review on Modification of Facet-Engineered TiO_2 for Photocatalytic CO_2 Reduction. *J. Photochem. Photobiol. C* **2018**, *36*, 24−47.
(156) Inoue, T.; Fujishima, A.; Konishi, S.; Honda, K. Photocatalytic Reduction of Carbon Dioxide in Aqueous Suspensions of Semiconductor Powders. *Nature.* **1979**, *277*, 637−638.
(157) Singh, S.; Modak, A.; Pant, K. K. CO_2 Reduction to Methanol Using a Conjugated Organic-Inorganic Hybrid TiO_2-C_3N_4 Nanoassembly. *Transactions of the Indian National Academy of Engineering.* **2021**, *6*, 395−404.
(158) Aguirre, M. E.; Zhou, R.; Eugene, A. J.; Guzman, M. I.; Grela, M. A. Cu_2O/TiO_2 Heterostructures for CO_2 Reduction Through a Direct Z-scheme: Protecting Cu_2O from Photocorrosion. *Appl. Catal. B: Environ.* **2017**, *217*, 485−493.
(159) Wei, Z. H.; Wang, Y. F.; Li, Y. Y.; Zhang, L.; Yao, H. C.; Li, Z. J. Enhanced Photocatalytic CO_2 Reduction Activity of Z-scheme CdS/$BiVO_4$ Nanocomposite with Thinner $BiVO_4$ Nanosheets. *J. CO_2 Util.* **2018**, *28*, 15−25.
(160) Wang, S.; Teramura, K.; Hisatomi, T.; Domen, K.; Asakura, H.; Hosokawa, S.; Tanaka, T. Optimized Synthesis of Ag-Modified Al-Doped $SrTiO_3$ Photocatalyst for the Conversion of CO_2 Using H_2O as an Electron Donor. *ChemistrySelect.* **2020**, *5*, 8779−8786.
(161) Miao, Y. F.; Guo, R. T.; Gu, J. W.; Liu, Y. Z.; Wu, G. I.; Duan, C. P.; Zhang, X. D.; Pan, W. G. Fabrication of In_2S_3/NiAl-LDH Heterojunction Photocatalyst with Enhanced Separation of Charge Carriers for Efficient CO_2 Photocatalytic Reduction. *Appl. Surf. Sci.* **2020**, *527*, 146792.
(162) Fu, J.; Zhu, B.; Jiang, C.; Cheng, B.; You, W.; Yu, J. Hierarchical Porous O-doped g-C_3N_4 with Enhanced Photocatalytic CO_2 Reduction Activity. *Small.* **2017**, *13*, 1603938.
(163) Gusain, R.; Kumar, P.; Sharma, O. P.; Jain, S. L.; Khatri, O. P. Reduced Graphene Oxide-CuO Nanocomposites for Photocatalytic

https://doi.org/10.1021/acsomega.3c02084
ACS Omega 2023, 8, 25649−25673

Conversion of CO_2 into Methanol Under Visible Light Irradiation. *Appl. Catal. B: Environ.* **2016**, *181*, 352−362.
(164) Li, Z.; Meng, X.; Zhang, Z. Recent Development on MoS_2-Based Photocatalysis: A review. *J. Photochem. Photobiol. C: Photochem. Rev.* **2018**, *35*, 39−55.
(165) Lv, R.; Terrones, H.; Elias, A. L.; Perea-Lopez, N.; Gutierrez, H. R.; Cruz-Silva, E.; Rajukumar, L. P.; Dresselhaus, M. S.; Terrones, M. Two-Dimensional Transition Metal Dichalcogenides: Clusters, Ribbons, Sheets and More. *Nano Today.* **2015**, *10*, 559−592.
(166) Zhou, W.; Zou, X.; Najmaei, S.; Liu, Z.; Shi, Y.; Kong, J.; Lou, J.; Ajayan, P. M.; Yakobson, B. I.; Idrobo, J.-C. Intrinsic Structural Defects in Monolayer Molybdenum Disulfide. *Nano letters.* **2013**, *13*, 2615−2622.
(167) Liu, P.; Choi, Y.; Yang, Y.; White, M. G. Methanol Synthesis from H_2 and CO_2 on a Mo_6S_8 Cluster: A Density Functional Study. *J. Phys. Chem. A* **2010**, *114*, 3888−3895.
(168) Santos, V. P.; van der Linden, B.; Chojecki, A.; Budroni, G.; Corthals, S.; Shibata, H.; Meima, G. R.; Kapteijn, F.; Makkee, M.; Gascon, J. Mechanistic Insight into the Synthesis of Higher Alcohols from Syngas: The Role of K Promotion on MoS_2 Catalysts. *ACS Catal.* **2013**, *3*, 1634−1637.
(169) Asadi, M.; Kumar, B.; Behranginia, A.; Rosen, B. A.; Baskin, A.; Repnin, N.; Pisasale, D.; Phillips, P.; Zhu, W.; Haasch, R.; Klie, R. F.; Kral, P.; Abiade, J.; Salehi-Khojin, A. Robust Carbon Dioxide Reduction on Molybdenum Disulfide Edges. *Nat. Commun.* **2014**, *5*, 1−8.
(170) Xie, Y.; Li, X.; Wang, Y.; Li, B.; Yang, L.; Zhao, N.; Liu, M.; Wang, X.; Yu, Y.; Liu, J.-M. Reaction Mechanisms for Reduction of CO_2 to CO on Monolayer MoS_2. *Appl. Surf. Sci.* **2020**, *499*, 143964.
(171) Wu, J.; Huang, Y.; Ye, W.; Li, Y. CO_2 Reduction: from the Electrochemical to Photochemical Approach. *Adv. Sci.* **2017**, *4*, 1700194.
(172) Meier, A. J.; Garg, A.; Sutter, B.; Kuhn, J. N.; Bhethanabotla, V. R. MoS_2 Nanoflowers as a Gateway for Solar-Driven CO_2 Photoreduction. *ACS Sustain. Chem. Eng.* **2019**, *7*, 265−275.
(173) Tu, W.; Li, Y.; Kuai, L.; Zhou, Y.; Xu, Q.; Li, H.; Wang, X.; Xiao, M.; Zou, Z. Construction of Unique Two-Dimensional MoS_2-TiO_2 Hybrid Nanojunctions: MoS_2 as a Promising Cost-effective Co-catalyst Toward Improved Photocatalytic Reduction of CO_2 to Methanol. *Nanoscale* **2017**, *9*, 9065−9070.
(174) Jung, H.; Cho, K. M.; Kim, K. H.; Yoo, H. W.; Al-Saggaf, A.; Gereige, I.; Jung, H. T. Highly Efficient Stable CO_2 Reduction Photocatalyst with a Hierarchical Structure of Mesoporous TiO_2 on 3D Graphene with Few-Layered MoS_2. *ACS Sustain. Chem. Eng.* **2018**, *6*, 5718−5724.
(175) Jia, P.-y.; Guo, R.-t.; Pan, W.-g.; Huang, C.-y.; Tang, J.-y.; Liu, X.-y.; Qin, H.; Xu, Q.-y. The MoS_2/TiO_2 Heterojunction Composites with Enhanced Activity for CO_2 Photocatalytic Reduction Under Visible Light Irradiation. *Colloids Surf, A Physicochem Eng. Asp.* **2019**, *570*, 306−316.
(176) Xu, F.; Zhu, B.; Cheng, B.; Yu, J.; Xu, J. 1D/2D TiO_2/MoS_2 Hybrid Nanostructures for Enhanced Photocatalytic CO_2 Reduction. *Adv. Opt. Mater.* **2018**, *6*, 1800911.
(177) Zhao, Y.; Cai, W.; Shi, Y.; Tang, J.; Gong, Y.; Chen, M.; Zhong, Q. Construction of Nano-Fe_2O_3-Decorated Flower-Like MoS_2 with Fe-S Bonds for Efficient Photoreduction of CO_2 under Visible-Light Irradiation. *ACS Sustain. Chem. Eng.* **2020**, *8*, 12603−12611.
(178) Dai, W.; Yu, J.; Deng, Y.; Hu, X.; Wang, T.; Luo, X. Facile Synthesis of MoS_2/Bi_2WO_6 Nanocomposites for Enhanced CO_2 Photoreduction Activity Under Visible Light Irradiation. *Appl. Surf. Sci.* **2017**, *403*, 230−239.
(179) Khan, B.; Raziq, F.; Bilal Faheem, M.; Umar Farooq, M.; Hussain, S.; Ali, F.; Ullah, A.; Mavlonov, A.; Zhao, Y.; Liu, Z.; Tian, H.; Shen, H.; Zu, X.; Li, S.; Xiao, H.; Xiang, X.; Qiao, L. Electronic and Nanostructure Engineering of Bifunctional MoS_2 Towards Exceptional Visible-light Photocatalytic CO_2 Reduction and Pollutant Degradation. *J. Hazard. Mater.* **2020**, *381*, 120972.
(180) Kim, R.; Kim, J.; Do, J. Y.; Seo, M. W.; Kang, M. Carbon Dioxide Photoreduction on the Bi_2S_3/MoS_2 Catalysts. *Catalysts.* **2019**, *9*, 998.
(181) Qin, H.; Guo, R.-T.; Liu, X.-Y.; Pan, W.-G.; Wang, Z.-Y.; Shi, X.; Tang, J.-Y.; Huang, C.-Y. Z-Scheme MoS_2/g-C_3N_4 Heterojunction for Efficient Visible Light Photocatalytic CO_2 Reduction. *Dalton Trans.* **2018**, *47*, 15155−15163.
(182) Sun, S.; An, Q.; Watanabe, M.; Cheng, J.; Ho Kim, H.; Akbay, T.; Takagaki, A.; Ishihara, T. Highly Correlation of CO_2 Reduction Selectivity and Surface Electron Accumulation: A Case Study of Au-MoS_2 and Ag-MoS_2 Catalyst. *Appl. Catal., B* **2020**, *271*, 118931.
(183) Ouyang, T.; Fan, W.; Guo, J.; Zheng, Y.; Yin, X.; Shen, Y. DFT Study on Ag Loaded 2H-MoS_2 for Understanding the Mechanism of Improved Photocatalytic Reduction of CO_2. *Phys. Chem. Chem. Phys.* **2020**, *22*, 10305−10313.
(184) Zheng, Y.; Yin, X.; Jiang, Y.; Bai, J.; Tang, Y.; Shen, Y.; Zhang, M. Nano Ag-Decorated MoS_2 Nanosheets from 1T to 2H Phase Conversion for Photocatalytically Reducing CO_2 to Methanol. *Energy Technol.* **2019**, *7*, 1900582.
(185) Lu, J.; Zhang, Z.; Cheng, L.; Liu, H. MoS_2-Wrapped $Mn_{0.2}Cd_{0.8}S$ Nanospheres Towards Efficient Photocatalytic H_2 Generation and CO_2 Reduction. *New J. Chem.* **2020**, *44*, 13728−13737.
(186) Wang, X.; He, J.; Mao, L.; Cai, X.; Sun, C.; Zhu, M. $CsPbBr_3$ Perovskite Nanocrystals Anchoring on Monolayer MoS_2 Nanosheets for Efficient Photocatalytic CO_2 Reduction. *Chem. Eng. J.* **2021**, *416*, 128077.
(187) Kumar, N.; Kumar, S.; Gusain, R.; Manyala, N.; Eslava, S.; Ray, S. S. Polypyrrole-Promoted rGO-MoS_2 Nanocomposites for Enhanced Photocatalytic Conversion of CO_2 and H_2O to CO, CH_4, and H_2 Products. *ACS Appl. Energy Mater.* **2020**, *3*, 9897−9909.
(188) Yin, S.; Li, J.; Sun, L.; Li, X.; Shen, D.; Song, X.; Huo, P.; Wang, H.; Yan, Y. Construction of Heterogenous S-C-S MoS_2/SnS_2/r-GO Heterojunction for Efficient CO_2 Photoreduction. *Inorg. Chem.* **2019**, *58*, 15590−15601.
(189) Wang, Y.; Zhang, Z.; Zhang, L.; Luo, Z.; Shen, J.; Lin, H.; Long, J.; Wu, J. C. S.; Fu, X.; Wang, X.; Li, C. Visible-Light Driven Overall Conversion of CO_2 and H_2O to CH_4 and O_2 on 3D SiC@2D MoS_2 Heterostructure. *J. Am. Chem. Soc.* **2018**, *140*, 14595−14598.
(190) Qiu, C.; Hao, X.; Tan, L.; Wang, X.; Cao, W.; Liu, J.; Zhao, Y.; Song, Y. F. 500 nm Induced Tunable Syngas Synthesis from CO_2 Photoreduction by Controlling Heterojunction Concentration. *ChemComm.* **2020**, *56*, 5354−5357.
(191) Alkanad, K.; Hezam, A.; Drmosh, Q. A.; Ganganakatte Chandrashekar, S. S.; AlObaid, A. A.; Warad, I.; Bajiri, M. A.; Neratur Krishnappagowda, L. Construction of Bi_2S_3/TiO_2/MoS_2 S-Scheme Heterostructure with a Switchable Charge Migration Pathway for Selective CO_2 Reduction. *Sol. RRL.* **2021**, *5*, 2100501.
(192) Geioushy, R. A.; Hegazy, I. M.; El-Sheikh, S. M.; Fouad, O. A. Construction of 2D MoS_2@ZnO Heterojunction as Superior Photocatalyst for Highly Efficient and Selective CO_2 Conversion into Liquid Fuel. *J. Environ. Chem. Eng.* **2022**, *10*, 107337.
(193) Wang, F.; Liu, D.; Wen, J.; Zheng, X. In-situ Sulfurized In_2S_3/MoO_3@MoS_2 Heterojunction for Visible Light-induced CO_2 Photoreduction. *J. Environ. Chem. Eng.* **2021**, *9*, 106042.
(194) Zheng, X.; Wang, H.; Wen, J.; Peng, H. In_2S_3-NiS Co-decorated MoO_3@MoS_2 Composites for Enhancing the Solar-light Induced CO_2 Photoreduction Activity. *Int. J. Hydrog. Energy.* **2021**, *46*, 36848−36858.
(195) Yu, F.; Jing, X.; Wang, Y.; Sun, M.; Duan, C. Hierarchically Porous Metal-Organic Framework/MoS_2 Interface for Selective Photocatalytic Conversion of CO_2 with H_2O into CH_3COOH. *Angew. Chem.* **2021**, *133*, 25053−25057.
(196) Li, H.; Sun, T.; Zhang, L.; Cao, Y. Improved Photocatalytic Activity of ZnO via the Modification of In_2O_3 and MoS_2 Surface Species for the Photoreduction of CO_2. *Appl. Surf. Sci.* **2021**, *566*, 150649.
(197) Singh, S.; Punia, R.; Pant, K. K.; Biswas, P. Effect of Work-function and Morphology of Heterostructure Components on CO_2

https://doi.org/10.1021/acsomega.3c02084
ACS Omega 2023, 8, 25649−25673

Reduction Photo-catalytic Activity of MoS_2-Cu_2O Heterostructure. *Chem. Eng. J.* **2022**, *433*, 132709.
(198) Li, P.; Hu, H.; Xu, J.; Jing, H.; Peng, H.; Lu, J.; Wu, C.; Ai, S. New Insights into the Photo-Enhanced Electrocatalytic Reduction of Carbon Dioxide on MoS_2-Rods/TiO_2 NTs with Unmatched Energy Bands. *Appl. Catal., B* **2014**, *147*, 912−919.
(199) Kim, M. S.; Don, W. J.; Hong, S. I.; Ri, M. I.; Yang, S. I. Photocatalytic Property of Two Dimensional Heterostructure MoS_2/WS_2 for Hydrogen Evolution via Water Splitting; a First Principles Calculation. *Int. J. Hydrog. Energy.* **2023**, *48*, 9371−9376.

https://doi.org/10.1021/acsomega.3c02084
ACS Omega 2023, 8, 25649−25673